Theses and Dissertations

Fall 2018

The effects of implant design variations on shoulder instability following reverse shoulder arthroplasty

Andrea Patricia Caceres
University of Iowa

www.manaraa.com

The Effects of Implant Design Variations on Shoulder Instability Following Reverse Shoulder Arthroplasty

by

Andrea Patricia Caceres

A thesis submitted in partial fulfillment
of the requirements for the Master of Science
degree in Biomedical Engineering in the
Graduate College of
The University of Iowa

December 2018

Thesis Supervisor: Professor Donald D. Anderson

ACKNOWLEDGEMENTS

ABSTRACT

Reverse shoulder arthroplasty (RSA) is performed to decrease pain and improve function and range of motion (ROM) primarily for patients with rotator cuff arthropathy, an arthritis of the shoulder secondary to rotator cuff insufficiency. However, RSA has suffered from high early to mid-term rates of complication, with instability being one of the most common. The shoulder biomechanics post-RSA depend on multiple factors such as implant geometry, positioning, and cuff integrity. This study built upon prior finite element (FE) analysis of RSA to investigate the effects of glenoid lateralization and retentive liner design on shoulder stability. A previously validated FE model was extended to model shoulder external rotation (ER) after implantation of the Zimmer Trabecular Metal RSA system. The FE model included the scapula bone with an implanted glenosphere implant, the humerus bone with implanted humeral sections of the RSA implant, and muscle tendons representing the subscapularis, infraspinatus, and deltoid. Six different models matched glenospheres in three cases of lateralization (2mm, 4mm, and 10mm) with two humeral poly liner designs (normal: 150° neck shaft angle or retentive: 155° neck shaft angle). Using Abaqus/Explicit FE software, the proximal ends of the soft tissues were pulled to their anatomical positions, and then fixed in space while the humerus was externally rotated 80° about the humeral long axis from a neutral position with the shoulder abducted 25°. The displacements, deltoid and subscapularis forces, impingement-free ROMs, and subluxation gap distances were recorded. Although greater glenosphere lateralization was associated with higher impingement-free ROM, larger deltoid and subscapularis forces developed. Deltoid tension contributes to shoulder stability and control, but elevated amounts of deltoid tension may contribute to scapular fractures and greater stress at impingement sites post-RSA. Further analysis such as inclusion of more anatomical features and additional motions may offer greater insight to orthopedic surgeons when planning for RSA insertion.

PUBLIC ABSTRACT

Shoulder motion is both stabilized and controlled by four rotator cuff muscles (the subscapularis, infraspinatus, supraspinatus, and teres minor), which act in a coordinated effort to rotate the arm around the glenohumeral joint. Patients with deficiency of the rotator cuff muscles and glenohumeral arthritis experience painful and severely limited glenohumeral motion, which if left untreated can lead to issues such as bone erosion. Reverse shoulder arthroplasty (RSA) allows these patients to regain motion by reversing the anatomical ball-and-socket joint. This enables the deltoid to raise the arm even in the face of the deficient rotator cuff. Although results have been promising, RSA is still a relatively new implant with variable implant design factors that work in tandem with any intact anatomy. This study used finite element analysis to model a shoulder joint with a Zimmer Trabecular Metal RSA system. The model included a fixed scapula with the scapular component of the implant attached, a movable humerus with inserted humeral component of the implant, and soft tissues including the subscapularis, infraspinatus, and deltoid. Six models were made combining different scapular implant lateralizations (2, 4, and 10mm) and humeral liner geometry (normal and retentive). External rotation was simulated on Abaqus Explicit for the shoulder model through 80°. Displacement between the humeral liner and glenosphere center of rotation, contact stress, and deltoid force were recorded and compared for the six models. Models where the shoulder component extended more outwardly from the body were associated with greater impingement-free range of motion at the cost of larger deltoid and subscapularis forces being developed. Although reasonable quantities of deltoid force enhance stability, elevated deltoid forces may contribute to scapular fractures and greater stress at impingement sites post-RSA. Inclusion of more anatomical features as well as other glenohumeral motions can expand upon this study. Ultimately, this modeling approach could provide valuable insights for surgeons to use in planning RSA surgery.

TABLE OF CONTENTS

LIST OF TABLES

LIST OF FIGURES

Figure 10. Radiological images before (a) and after (b) RSA for three cases. Indications for RSA tend to fall into three categories: glenohumeral arthritis with rotator cuff deficiency (1a), proximal humeral fractures (2a), and revision for failed arthroplasty (3a). Section 1 a/b shows cuff tear arthroplasty and severe bone loss due to prolonged cortisone use treated

ix

x

CHAPTER 1: INTRODUCTION

Reverse shoulder arthroplasty (RSA) restores pain-free function and range of motion (ROM) for patients with irreparable rotator cuff tears and glenohumeral arthritis (Fig. 1). Since its FDA approval in 2003, RSA has increased in popularity, accounting for 33% of all shoulder arthroplasties performed in the USA during 2007 [34, 59]. Its success in relieving pain and restoring function has allowed it to become a valid complement to hemi and total shoulder arthroplasties. In turn, this has expanded the scope of candidates for RSA beyond elderly patients (70 years or older) with significant rotator cuff tears to include younger populations with rotator cuff deficiency, rheumatoid arthritis, proximal humeral fractures or previously failed shoulder implants [4-10, 14, 15, 19, 21, 23, 25, 26].
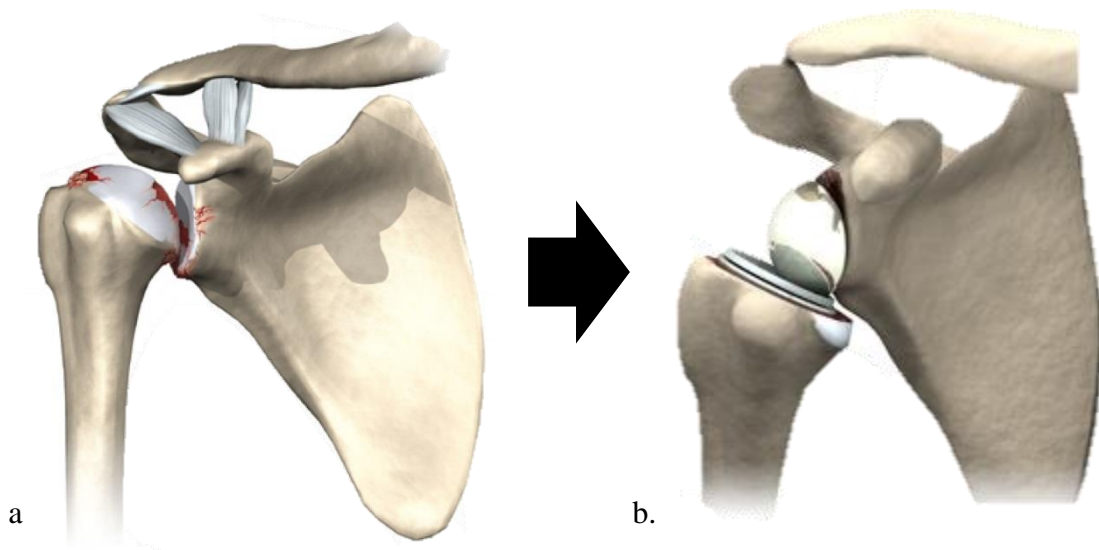
Figure 1. For patients with rotator cuff tears and osteoarthritis (a), reverse shoulder arthroplasty (b) reverses the traditional ball-and-socket joint to enable the deltoid to control motion instead of the rotator cuff. Images curtesy of Eorthopod.com < https://eorthopod.com/reverse-shoulder-arthroplasty/>

RSA reverses the ball-in-socket design of the native shoulder by implanting a hemispherical component onto the lateral glenoid surface and a cup-stem component onto the proximal portion of the humerus (Fig. 1). This distinguishes RSA from the other two shoulder arthroplasties, hemi arthroplasty and total shoulder arthroplasty (TSA), which replicate the native anatomy of the shoulder (Fig. 2). Moving the center of rotation both distally and medially creates a larger moment arm, which in turn, allows the deltoid muscle to move the humerus with increased efficiency and stability in cases where the four rotator cuff muscles (subscapularis, infraspinatus, supraspinatus, and teres minor) are compromised [53, 59]. Despite ongoing advances to RSA, high complication rates have persisted. Improved implant systems need to address the mechanical tradeoffs that accompany variable implant design and patient anatomy.

a. Hemi   b. Total   c. Reverse

Figure 2. a) Zimmer Biomet's Anatomical Shoulder Combined Hemi Arthroplasty, b) Zimmer Biomet's Comprehensive Total Shoulder system, c) Zimmer Biomet's Trabecular Metal RSA system (used for this study). Images of curtesy of Zimmer Biomet <http://www.zimmer.com/>

2

Finite element (FE) analysis is becoming an increasingly reliable tool to efficiently model joint mechanics and predict wear patterns prior to insertion. This study used FE analysis through Abaqus Explicit to investigate how geometrical variations such as glenosphere lateralization and liner type in RSA design can affect the biomechanics of the shoulder. Knowledge of post RSA biomechanics can allow surgeons to make educated decisions concerning implant specifications that will contribute to better success rates post RSA insertion.

1.2 ANATOMY

The shoulder is the most mobile joint in the human body, but it comes at the cost of joint stability that tenuously relies on muscle action. Functional ROM, the amount of movement needed for active daily living such as eating, bathing, and dressing, varies with type of glenohumeral (ball and socket) motion. Studies have found that average ROM needed for active daily living (ADL) to be the following: abduction (112° [42] to 121° [52]), adduction (116° [45]), flexion (99° [52] to 118° [42]), extension (67° [42] to 68° [32]), internal rotation (85° [52] to 110° [2]), and external rotation (60° [52] to 62° [2]) at the glenohumeral joint. Although ADL threshold values fall below the normal upper limits of glenohumeral motion for healthy adults, individuals with rotator cuff tears often fail to meet ADL lower bounds, reducing their quality of life (Fig. 3). Actions such as brushing one's hair and reaching for the superior portion of the spine required the highest ROMs for abduction and flexion, while reaching for the lower back required the highest external rotation and extension [45]. Articulations from the sternoclavicular and the acromioclavicular joints, along with gliding motion at the scapulothoracic juncture, also affect overall shoulder motion, with the scapulothoracic motion contributing roughly a third of normal shoulder adduction.

3
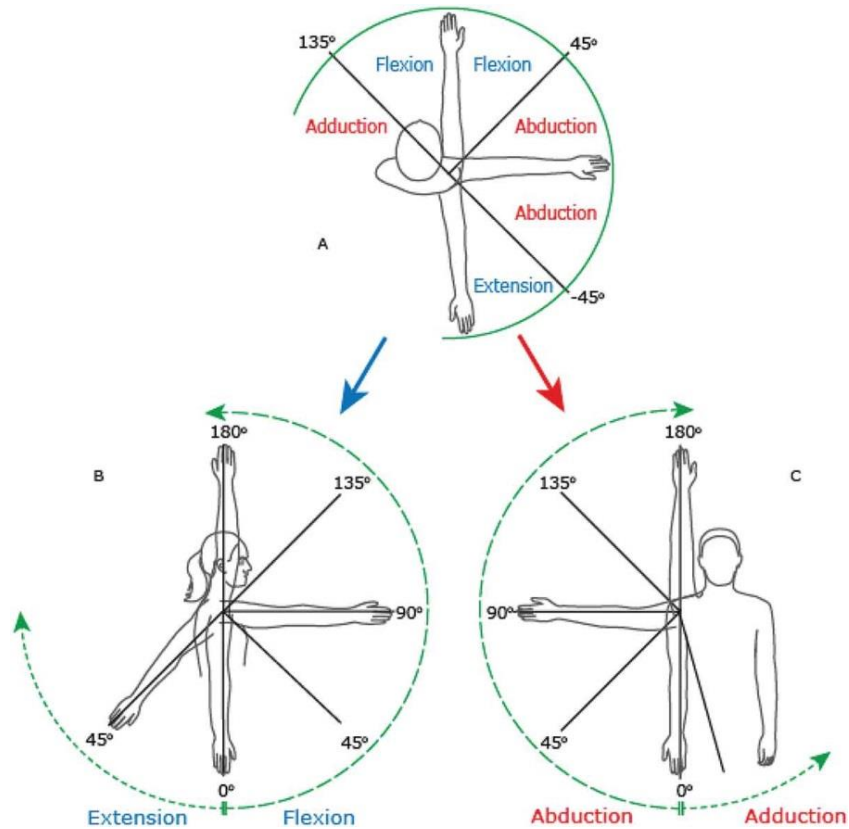
Figure 3. Normal, upper limits of motion for extension/flexion and ab/adduction. ADL values fall below these limits, but patients with rotator cuff arthropathy are unlikely to meet minimal ADL glenohumeral motion values. [45]

The rotator cuff plays an essential role in providing control and stability during motion. The complex, multilayer structure of interconnected tendons, cartilage, and other tissues allows for multiple combinations of controlled motion [54] (Fig. 4). The four rotator cuff muscles work in a complementary fashion to effect motion. The largest of the four muscles, the subscapularis, contributes to internal rotation, the infraspinatus and teres minor contribute to external rotation, and the supraspinatus aids in humeral abduction. Motion is also limited by the glenohumeral ligament and the infeior glenohumeral ligament complex, as well as the presence of soft tissue acting as physical barriers for motion.

4
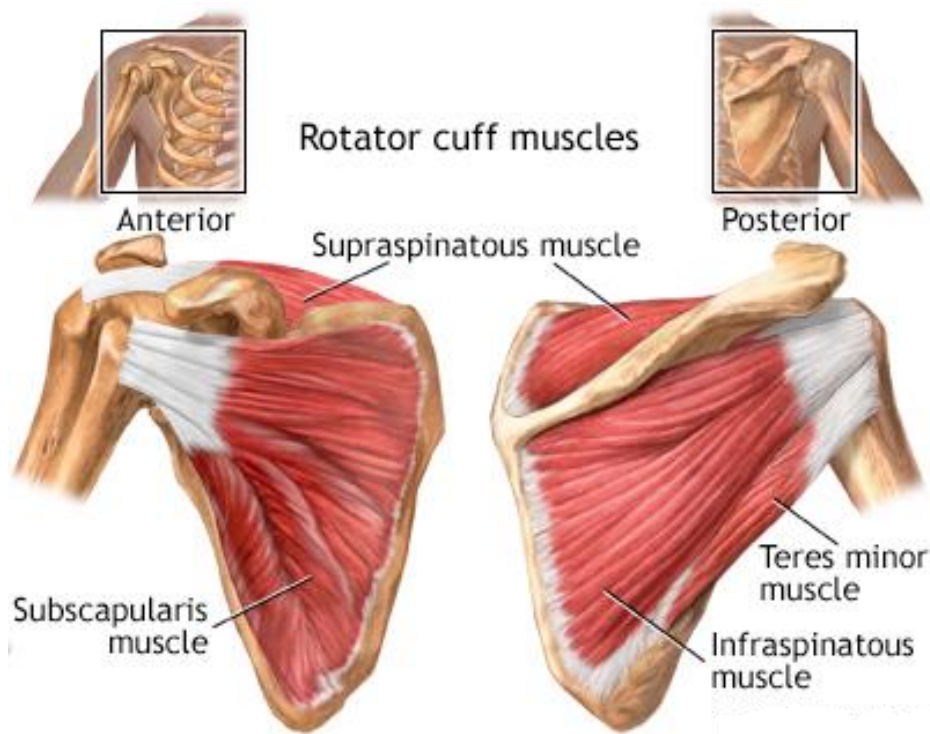
Figure 4. Anterior and posterior view of the left shoulder. The four rotator cuff muscles provide stability and control during glenohumeral articulations. Image curtesy of Medline plus < https://medlineplus.gov/ency/imagepages/19622.htm>.

Due to rotator cuff deficiencies, candidates for RSA experience eccentric, unstable glenohumeral motions that create pathological wear patterns, which are not only painful and damaging to the bone, but may also elevate risks of scapular notching, instability, and wear along the impinging surfaces [59]. Additionally, absence of soft tissue surrounding the glenohumeral joint allows the humeral head to migrate superiorly, leading to acromial erosion or acetabularization [59].

The nature of the cuff deficiency varies considerably across cuff tear arthropathy patients, with implications for shoulder stability and function after RSA. Interestingly, cuff tears are more prevalent in females, but this may be due to women having, on average, longer lifespans than

men. Absence of rotator cuff tissue, as well as glenohumeral arthritis, not only severely limits ROM below ADL thresholds, but also begets compensatory movements that can further alter joint kinematics/biomechanics. Regardless of muscle deficiency, elderly populations showed reduced functional ROM compared to younger populations [35]. Due to the mismatch between the large humeral head and shallow glenoid socket, the stability of the shoulder may become more easily compromised [36]. Variability of the natural anatomy of the shoulder stresses the need for patient-specific sizing and modularity to address mechanical tradeoffs when reverse shoulder arthroplasty is needed [27].

1.3 HISTORICAL AND CURRENT INVESTIGATIONS

The earliest reports of shoulder arthroplasty date back to the late 1800s, with Themistocles Gluck designing the first prosthetic shoulder in 1891, and Jules Emile Péan performing the first shoulder arthroplasty insertion in 1893 [11, 21, 63]. Charles Neer played a pioneering role in reverse shoulder arthroplasty, experimenting with geometrical changes to shoulder arthroplasty in the 1950s as a response to poor return in functionality observed in patients with rotator cuff deficiencies [28, 43]. Neer observed cuff tears, before and after RSA, as well as types of deficiency, but was unable to successfully address the issue. Arthroplasty experiments included changing the size of the ball and its location, alternating between reverse and anatomical configurations, inclusion of axial rotation, as well as constrained prosthesis designs [21, 31, 43]. Although patients regained ROM for several iterations of Neer's RSA design, instability, among other complications, was still prevalent. Despite being unsuccessful, these experiments set the stage for the modern RSA system.

Current RSA designs stem from Dr. Paul Grammont's reverse shoulder system initially tested on eight subjects [21, 28]. As opposed to the anatomical shoulder, the device featured: a stable prosthesis; combination of a convex weightbearing part articulating with a concave support; sphere center located at the glenoid neck; and a medial and distal movement of the center of rotation (COR) [21]. Comparisons of COR can be seen in Fig. 5. The first iteration of the DELTA RSA system also featured modular components. Revisions were added to address loosening and breakage of the glenoid component observed in the initial device, creating the Delta III RSA. The DELTA III included a central peg with screws at the glenoid to counteract shear forces and increase abduction [4]. Even with improvements, high complication rates persisted, most notably scapular notching, limited external motion, and decreased deltoid efficiency associated with the new medialized center [59].
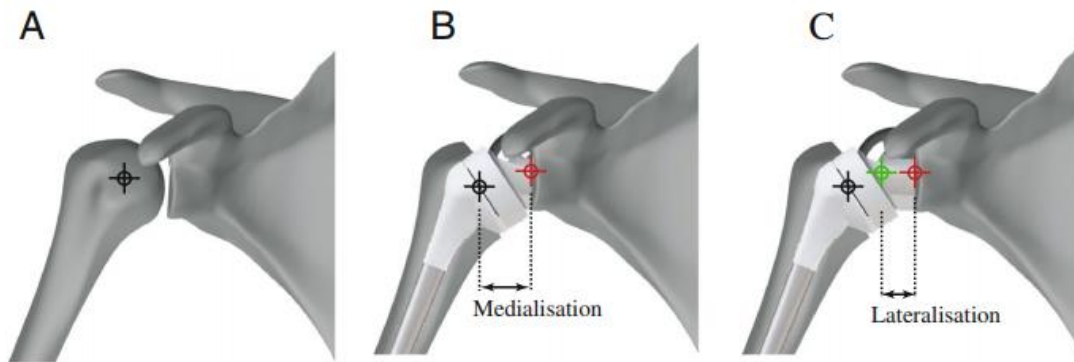
Figure 5. "Diagram illustrating joint center of rotation location for the anatomical shoulder (a), reverse shoulder (b), and reverse shoulder with a lateral-offset glenoid component (c). Medialization after reverse total shoulder arthroplasty is shown, as well as lateralization due to a lateral-offset glenoid component. Black, red, and green bell's eyes indicate joint center of rotation position for the anatomical." [1]

7

The introduction of modularity and associated tradeoffs to RSA design have been a focal point for RSA research in the last two decades. Inserting the glenoid baseplate on the inferior glenoid margin instead of the center of the glenoid reduces impingement of the humerus on the inferior glenoid ridge [1]. Although several RSA variables have been studied individually, questions arise when combining several variables such as glenoid offsets and humeral offsets seen in Fig. 6, or glenoid lateralizations and different humeral liner types as seen in this study. Lateralizing the glenoid component decreases the deltoid lever arm and increases forces developed by the deltoid. This allows greater range of motion at the cost of producing instability and elevated risk of dislocation. The effects of lateralization on the soft tissue surrounding the glenohumeral joint still need to be better understood, and there are limited FE models that adequately incorporate soft tissue supports to motion. Acromion impingement and fractures have been linked to elevated forces transferred to the deltoid post RSA.
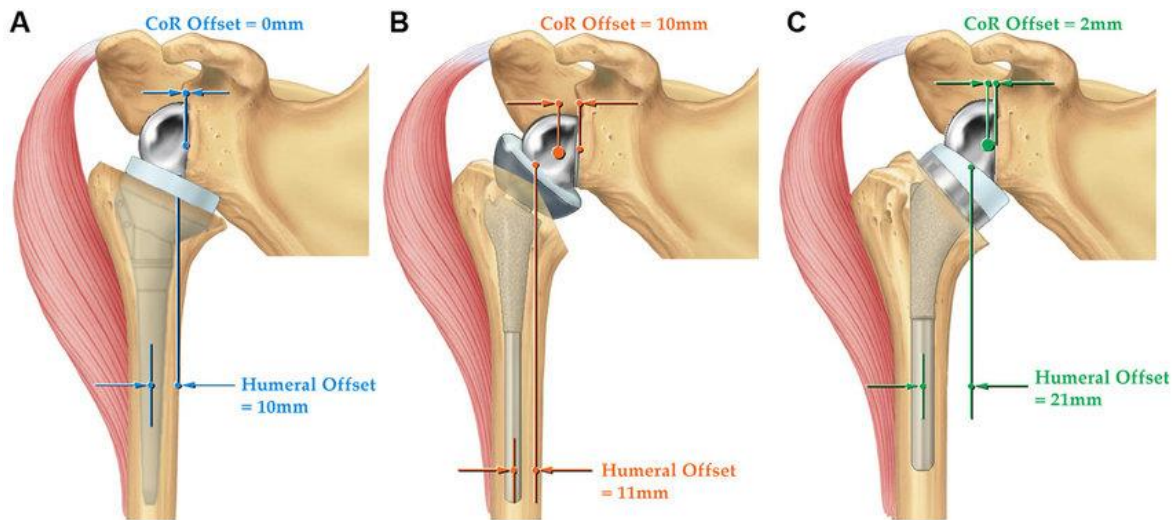
Figure 6. "Drawings showing the differences among 3 different types of reverse total shoulder arthroplasty and the location of both the center of rotation (CoR) and the relative lateral displacement of the humerus based on the design of the implant: Grammont Delta III Reverse Shoulder, Depuy, Warsaw, IN (medial glenoid and medial humerus) (A), RSP Reverse Shoulder, DJO Surgical, Austin, TX (lateral glenoid and medial humerus) (B); and Equinoxe Reverse Shoulder (medial glenoid and lateral humerus) (C)." [22]

1.4 FINITE ELEMENT ANALYSIS

One of the most critical advances in biomechanical research has been implementation of computer modeling software to determine anatomical interactions (Fig. 7) while avoiding invasive techniques. Computer software reliant on finite element analysis (FEA) can be used to solve multiple features about the model in question including force, heat, and stress distributions, failure dynamics, and nodal displacements, given certain conditions. The finite element method has been used since the 1940s and relies on division of complex mechanical structure into simple components called elements [62]. Originally used to solve elasticity and structural problems by giving numerical solutions to nonlinear set ups, FE methods have gained widespread use in various fields.
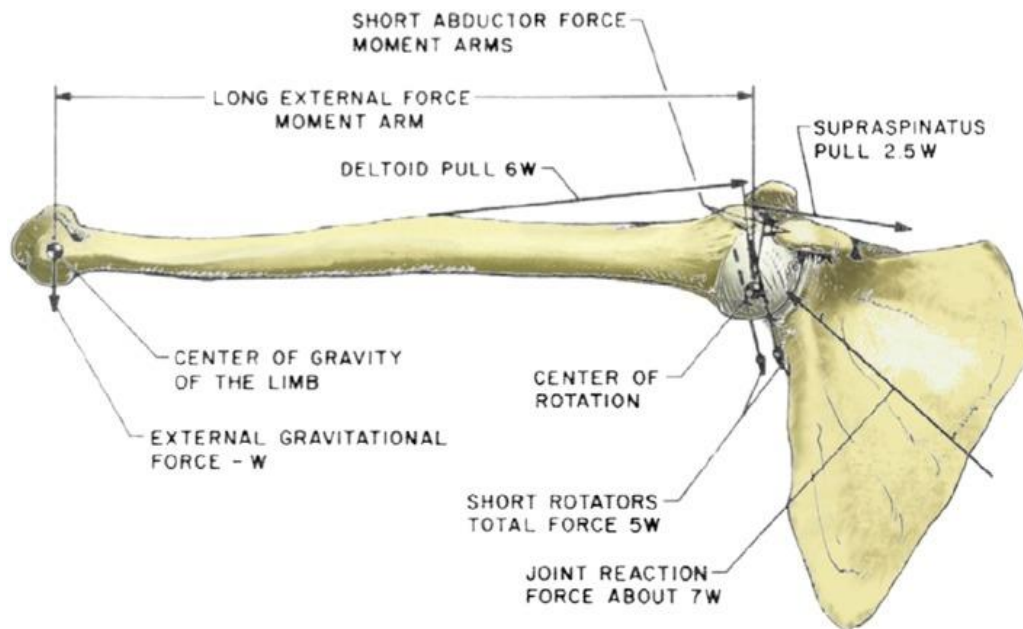
Figure 7. Finite element analysis allows biomechanical forces, such as those found at the glenohumeral joint, to be modeled. Shown here are glenohumeral forces at 90° [62].

9

Current biological applications of FEA involve an amalgamation of various resources. Typically, the anatomical geometry is captured through the segmentation of radiographic images, most often CT or MRI scans. The segmented geometry is then meshed, mechanical properties from the literature are applied as well as boundary conditions, and finally FE algorithms are used to solve the model. Given the complex structures and varying material properties of the shoulder, modeling its mechanical behavior has proven more difficult, and scientists rely on assumptions and simplification in order to model the system effectively [60, 62]. This is especially true for the soft tissues whose integrity is inconsistent in candidates for rotator cuff surgery.

Most shoulder models represent soft tissue as pulleys along the muscle lines of actions, which may model stability to a certain point, but neglect factors such as wrapping, contact, and nuances in stress distribution on the tissue. This is because of the difficulty to segment soft tissue from radiographic scans and implement them into the model. Simplification of geometries, as well as only modeling specific parts of the glenohumeral joint have been the necessary to reduce computational load [60]. Recent attempts have been made to use continuous 3D elements to model rotator cuff muscles and the labrum for healthy specimens using static FE solvers [61, 63]. Inclusion of continuous element musculature for RSA in dynamic modes can enable more accurate representations of the shoulder system and accompanying biomechanical phenomena [49, 62].

Work in the University of Iowa Orthopaedic Biomechanics laboratory has aimed to add complexity to RSA shoulder models to better investigate aspects related to scapular notching and instability associated with modern RSA implant systems. Prior finite element work related to this line of research (led by Dr. Vijay Permeswaran as part of his PhD dissertation studies) modeled Tornier's Aequalis Ascend Flex RSA system and focused on evaluating liner version and glenoid

lateralization using a bony increased offset (BIO) lateralizing cylinder fixed centrally on the glenoid. Initial FE models relied on simple spring and cable representations of soft tissue, later evolving into multiple cables to represent each rotator cuff muscle, until eventually introducing continuous element representations for soft tissues (Fig. 8).
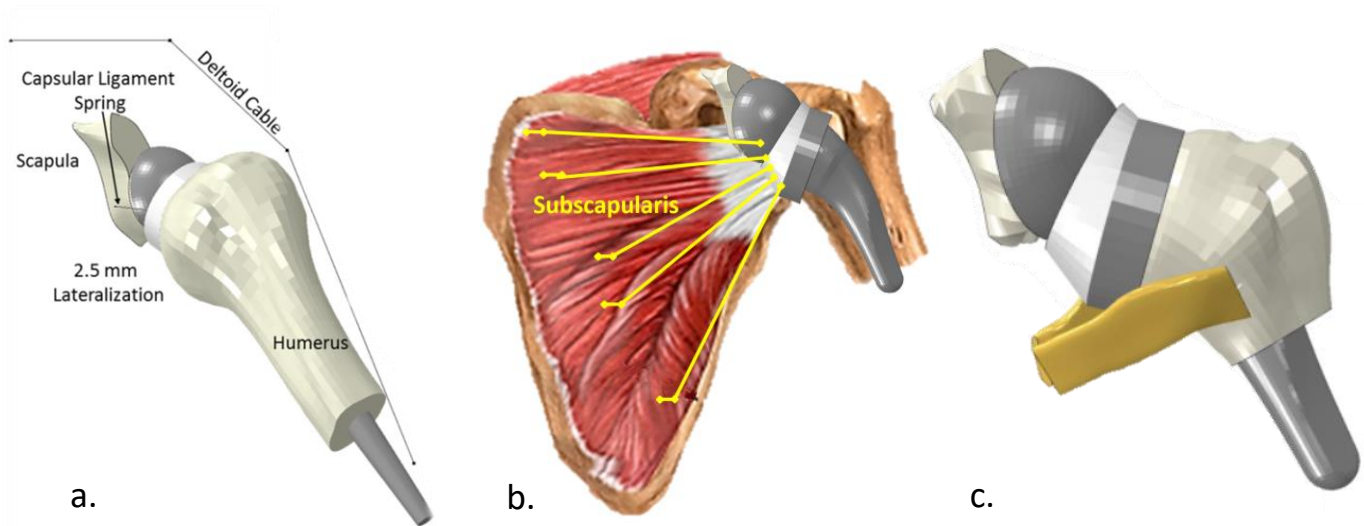
Figure 8. Prior in-house research initially relied on minimal spring & cable representations of soft tissue (a) [48], later replacing springs with multi-cable soft tissue representations (b), and finally experimenting with continuous element soft tissue models (c) [48].

1.5 INSERTION TECHNIQUES

Several surgical approaches exist to address muscle deficiency with or without RSA. Orthopedic surgeons currently rely on their best judgement to accommodate variable cuff deficiencies as well as for insertion of the RSA system. Muscle transfer is a surgical option considered in certain patients to restore cuff support, but it is difficult to predict before surgery when it may be needed [24, 33, 43]. Oftentimes RSA is performed on failed muscle transfers for lack of gained mobility.

11

Of the three main RSA surgical approaches, the deltopectoral is preferred because it is associated with fewer complications and allows better visualization of the area than the superolateral approach, which is especially important in revision operation (Fig. 9). The deltopectoral procedure runs an increased risk of subscapularis dysfunction as well as damage to the musculocutaneous nerve, cephalic vein, axillary nerve, and anterior circumflex humeral artery. Incision runs from the inferior border of the clavicle and transverses on the coracoid process, heading towards deltoid along the deltopectoral groove [4, 40]. Preservation of the cephalic vein is critical as damage to it can result in edema, denervation, loss of control, and loss of sensation in the area [4].
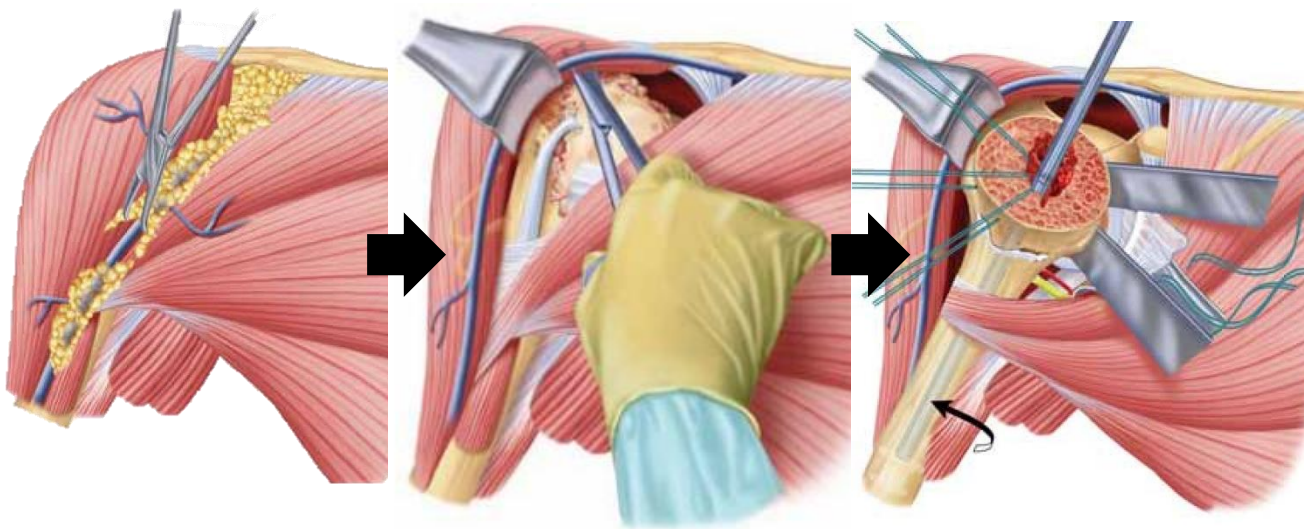
Figure 9. Dissection is along the deltopectoral groove of the deltoid using the deltopectoral approach [38].

The superolateral (deltoid splitting) approach carries risks of damaging the deltoid, subscapularis, and axillary nerve, as well as increased risk of badly positioning the glenoid component making the superolateral approach less common. The large visibility of the

12

glenohumeral joint makes this approach favorable for patients with acromion fractures. In some cases, a rotator cuff-sparing approach based on the deltopectoral approach has been used, which involves re-attaching any musculature disturbed during surgery. Unfortunately, this is reliant on limited rotator cuff deficiency, a primary indication for RSA [13].

1.6 PRE- & POST-OPERATIVE PERSPECTIVES

Patients in need of RSA typically suffer from the following: rotator cuff deficiencies with accompanying osteoarthritis, severe proximal humeral fractures, or previously failed arthroplasty (Fig. 10) [7, 9, 26, 51, 55, 65]. In all cases, the biomechanical fulcrum for elevation is lost and unable to be restored with rotator cuff surgery or other arthroplasties. Patients with cuff deficiency and osteoarthritis are unable to abduct the humerus above the horizontal plane of the shoulder regardless of treatment to the muscles such as strengthening and surgical interventions. Beyond the pain these patients exhibit, some may also exhibit anterosuperior escape of the humeral head, and other irregularities when attempting glenohumeral articulations [8, 10]. Deficiency in the anterosuperior or postero-superior cuff, in particular, leads to subluxation and produces increased risk of pseudoparalysis if left untreated [14]. Hemi or total shoulder arthroplasty are unable to resolve anterior-superior escape or reproduce rotator cuff force couples, resulting in loss of motion and function [26]. Reverse shoulder arthroplasty restores mobility by moving the center of rotation medially on the glenoid, which allows elevated deltoid forces. Additionally, lowering the humerus places the deltoid under tension, further stabilizing the joint [26].

13

Figure 10. Radiological images before (a) and after (b) RSA for three cases. Indications for RSA tend to fall into three categories: glenohumeral arthritis with rotator cuff deficiency (1a), proximal humeral fractures (2a), and revision for failed arthroplasty (3a). Section 1 a/b shows cuff tear arthroplasty and severe bone loss due to prolonged cortisone use treated before and after RSA [9]. Section 2a/b shows a proximal humeral fracture with a failed ORIF before and after RSA [55]. Section 3a/b shows a failed TSA 10 years after insertion before and after revision to RSA [51].

Reverse shoulder arthroplasty is also used to treat patients with severe proximal humeral fractures (Fig. 10 a/b) [51]. Although traditionally patients with acute proximal humeral fractures

www.manaraa.com

were treated with hemiarthroplasties, several recent studies have shown that RSA creates more favorable outcomes with quicker recovery times because RSA depending less on tuberosity healing and rotator cuff integrity [12, 17, 26]. Specifically, patients with proximal humeral fractures that opted for RSA instead of hemi arthroplasty were seen to have greater flexion at the cost of less external rotation [20]. Other studies have cautioned that RSA insertion for acute humeral fractures may elevate the risk of scapular notching long term as well as tuberosity displacement, and periprosthetic calcifications. Likewise, patients with malunited proximal humeral fractures show high complication rates in all three implant options.

Recently, studies have shown RSA leads to faster recovery times for patients with accompanying humeral fractures compared to hemi arthroplasty [26]. Positive results have also been seen in patients with pre-operative pseudoparalysis and patients with failed rotator cuff surgery [6, 26, 29, 33]. Since the purpose of RSA is to replace the rotator cuff force with an elevated use of the deltoid, patients with deltoid weakness or deficiency may not recover range of motion and may even reduce functionality from its pre-insertion state. Axillary nerve damage is another contraindication, as this would decrease the amount of control on the area [26].

In addition to scapular notching (Fig. 11), instability accounts for 38% of all complications due to unbalanced force coupling mechanisms associated with rotator cuff deficiency [10, 13, 41, 64] (Fig. 12). Scapular notching is produced by impingement between the humeral polyethylene component and the inferior lateral portion of the scapula. Repeated contact between the two surfaces gradually wears away the scapular bone leading to glenoid loosening that may require revision (Fig. 13). Infection and inflammation are among the other most common post RSA complications, and are common complications for any implant post insertion.

15
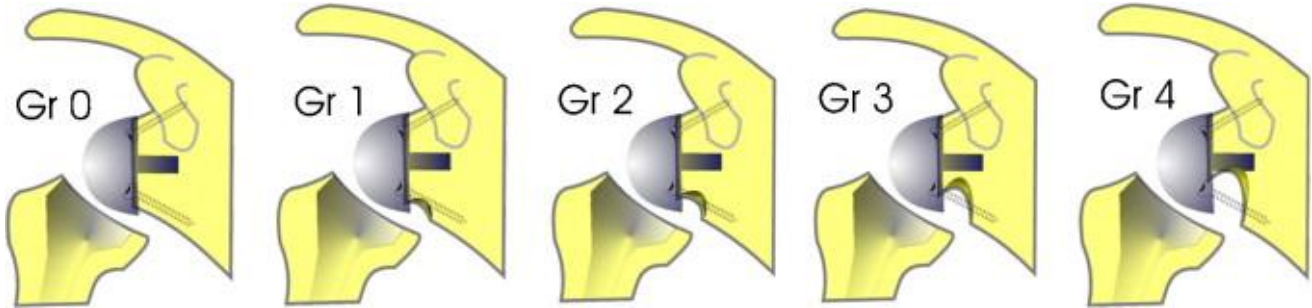
Figure 11. Repeated impingement between the humeral liner and inferior scapula produces scapular notching which propagates if left untreated, eventually leading to glenoid component loosening and possible revision. Shown above is the Nerot-Sirveaus scapular notching classification to determine severity [16].

Figure 12. "Radiological anteroposterior view of scapular notching grade 2 (according to Nérot classification) at three (a) and eight years (b) after reverse total shoulder arthroplasty (RTSA) (Delta III)" [15].
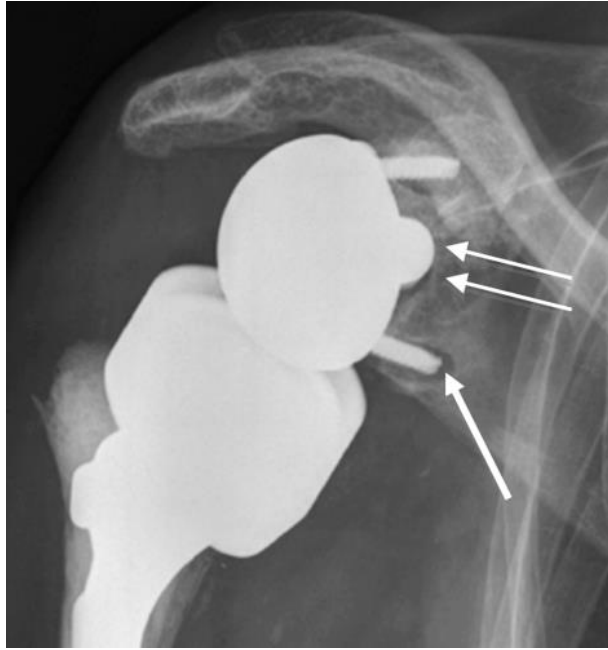
Figure 13. **"**Glenoid component loosening six months after reverse total shoulder arthroplasty (RTSA) for irreparable rotator cuff arthropathy and osteoarthritis. Radiolucency is seen particularly around the inferior screw (arrow) and around the glenoidal implant central peg (double arrow)" [14].

1.7 PURPOSE

Despite instability being one of the most prevalent complications in patients with RSA, many prior computational studies on the shoulder have stopped analysis once impingement occurs, making it impossible to study post impingement instability. Other shoulder FE models have reduced the complexity or omitted peripheral structures such as soft tissue due to extra amount of time needed to run models, and difficulty accurately capturing the geometry and characteristics. The few dynamic finite element RSA shoulder models that have included soft tissues have primarily relied on linear pulleys or springs along the line of action for a muscle group as a stand in for the whole soft tissue. Previous work at the University of Iowa

17

Orthopaedic Biomechanics laboratory involved introducing continuous element representations of soft tissues to models investigating implant geometry variations in RSA [46, 47, 48].

Building on prior dynamic finite element analysis of RSA [46, 47, 48], the goal of this study was to investigate the effects of glenoid lateralization and liner design on shoulder stability for a new implant system from Zimmer Biomet. Other additions to the modeling approach were the inclusion of superior elements of the scapula (the acromion and coronoid process) along with the introduction of an explicit deltoid muscle structure.

One of the ways to characterize instability is by quantifying the subluxation post impingement, calculated as the magnitude of displacement between the centers of rotation of the poly liner and glenosphere (Fig. 14). If left untreated, instability may lead to dislocation and revision surgery. Alternatively, elevated amounts of tension specifically in the deltoid may lead to acromial fractures. Inclusion of continuous element representations of soft tissues such as the lateral portion of the deltoid, subscapularis, and infraspinatus allowed investigation of the forces in these soft tissues as well as their role in ER motion. External rotation was chosen because impingement is most common during this motion [48]. This study investigated how different combinations of glenoid lateralization and liner type affected subluxation, deltoid force, subscapularis force, impingement location, and impingement-free ROM while also adding complexity to the model. This study also investigated how soft tissue inclusion affected instability at the glenohumeral joint by using continuous element representations aligned to their corresponding rotator cuff muscle location.

18
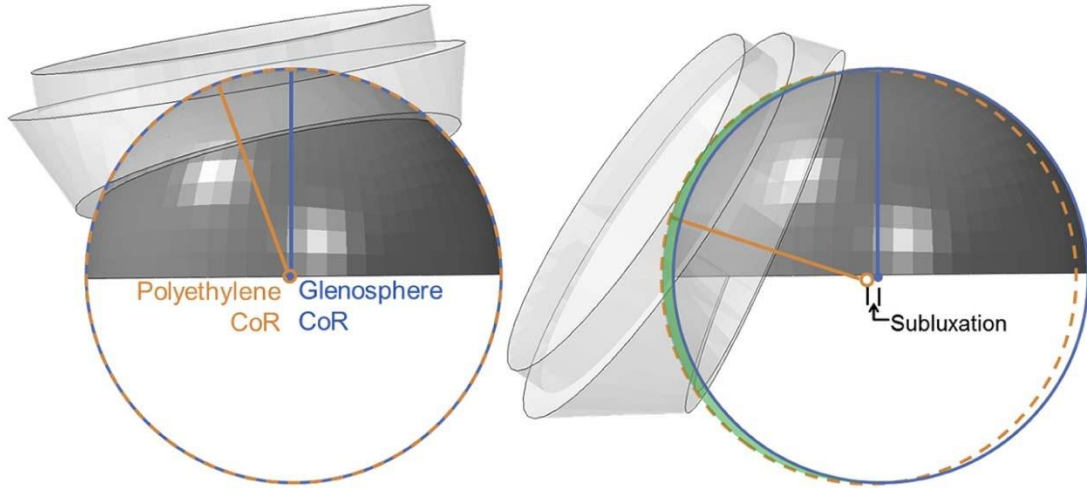
Figure 14. Subluxation is defined as the distance between the polyethelene liner COR and the glenosphere COR [47, 48].

CHAPTER 2: METHODS

2.1 MODEL CREATION

The scapula, humerus, and central band of the deltoid were segmented using CT scans from the female dataset of the Visible Human Project (NIH), while the subscapularis and infraspinatus were taken from MRI scans from a previous study [46]. Scans were run through an image threshold-based segmentation process and then adjusted manually using Seg3D (Scientific Computing and Imaging Institute, CIBC) (Fig. 15). Seg3D is an open source segmentation program developed by MIT that creates 3D volumetric renderings from 2D orthogonal medical image (in this case, CT) slices. Beginning with an adjustable threshold feature, layers were then edited using features such as hole-filling, erosion, and manual painting to specify the boundaries of individual bones or soft tissues.

Axial Plane Slice

Sagittal Plane Slice   Coronal Plane Slice   3D Volumetric Rendering
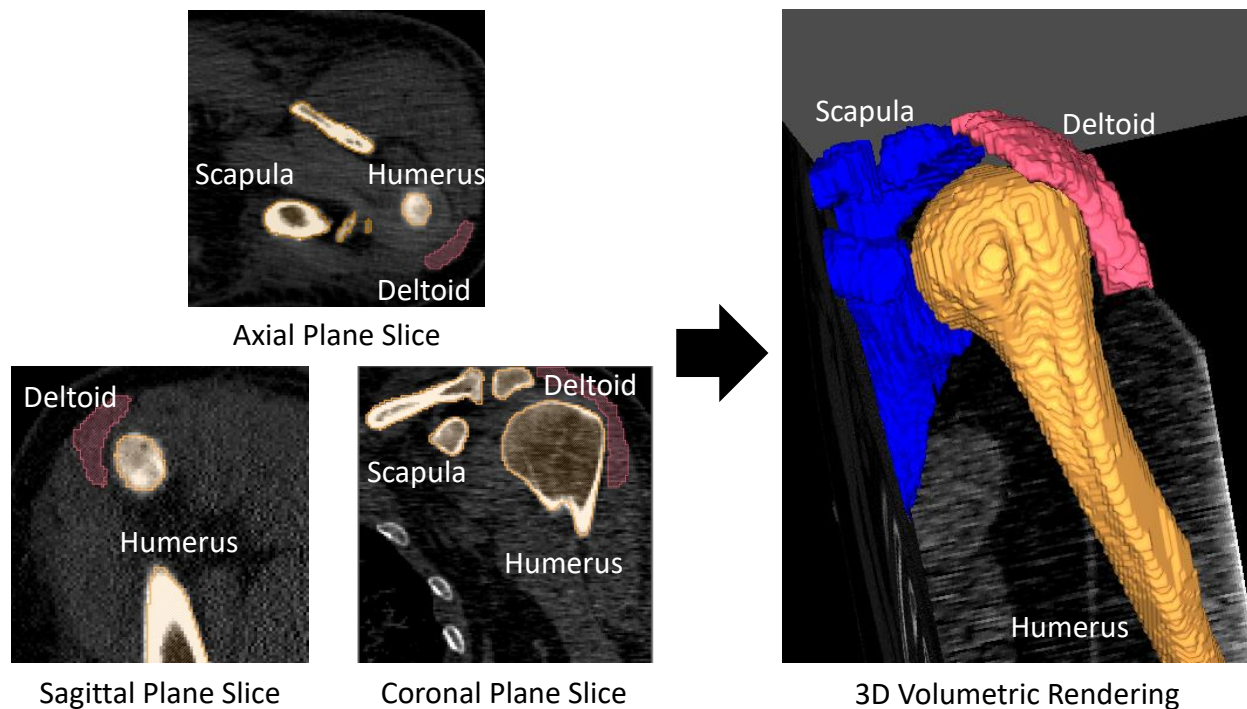
Figure 15. Seg3D combines 2D CT slices from the axial, sagittal, and coronal planes into 3D volumes of the anatomical topography. Shown above are axial, sagittal, and coronal plane slices (left), and the volumetric representation of the combined layers.

Zimmer Trabecular Metal RSA (Zimmer Biomet) implant components were laser scanned using a Faro Edge Scanarm (FARO Technologies) and Geomagic Design X software (3D Systems). The Faro Edge Scanarm is a 7-axis, 3D laser scanner that uses laser stripe triangulation to digitize object surfaces without direct contact [58] (Fig. 16). In order to reduce the reflectivity of the implant, metallic surfaces were sprayed with an opaque talc coating prior to scanning. Implant parts were kept in place with putty on a stable, flat surface as the laser scanner manually revolved around the object. Accuracy of volumetric measurement is 0.034mm while single point repeatability is 0.024mm according to the manufacturer [58], although two studies have found uncertainties of 0.2 [57] and 0.1 [37]. 36mm and 40mm glenospheres, long (4.5mm) and short (2.5mm) lateralized baseplates, a 10x130mm RSA stem, standard & retentive liners, and 9mm humeral spacer had two to five scans taken per individual part that were then combined

21

to create a 3D surface rendering. The scan points were smoothed and aligned to the shoulder

system using Geomagic Studio software (3D Systems) (Fig 17).

Figure 16. The Faro Edge Scanarm uses a 7-axis 3D laser scanner to digitize the geometry of an object to point based cloud registration software [17].

a.　　　　　　　　　　　　b.　　　　　　　　　　　　c.
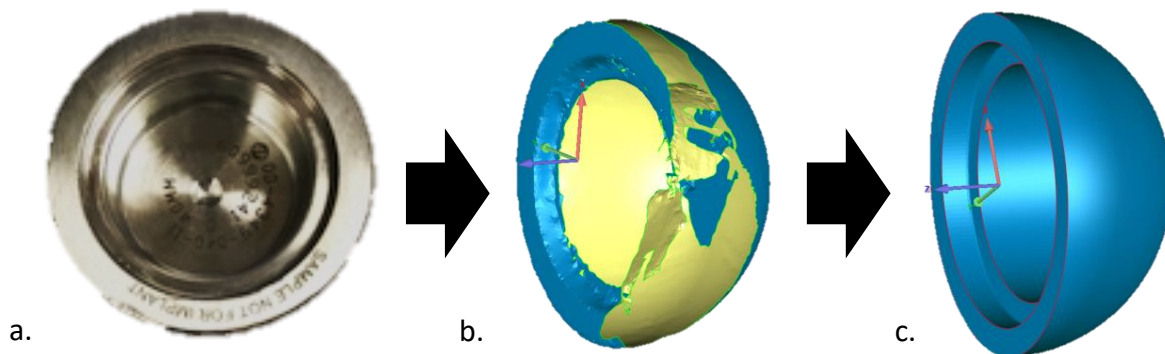
Figure 17. A 40mm CoCr glenosphere from the Zimmer Trabecular Metal RSA system (a), FaroArm laser scan of the glenosphere rendered on Geomagic Design X (b), and edited rendering on Geomagic Studio after fitting simple geometry (c).

2.2 EDITING, INSERTION, AND ALIGNMENT

The implant surfaces produced in Geomagic Studio from the raw laser scan data, suitably combined and cleaned up, were further processed to produce clean geometric models that facilitate the FE analysis. Geometric primitives (hemispheres, cylinders, etc) were fit to the 3D surface geometries of the implant components within Geomagic Studio and assembled to produce more accurate, crisp representations of their real-life counterparts (Fig. 17) (Fig. 18). The humeral bone, scapula, and deltoid were also edited in Geomagic to provide smoother surface geometries that were free of any holes or anomalous features. The deltoid anatomy was approximated by more simplified basic geometry, as had previously been done for the subscapularis and infraspinatus [47, 48].
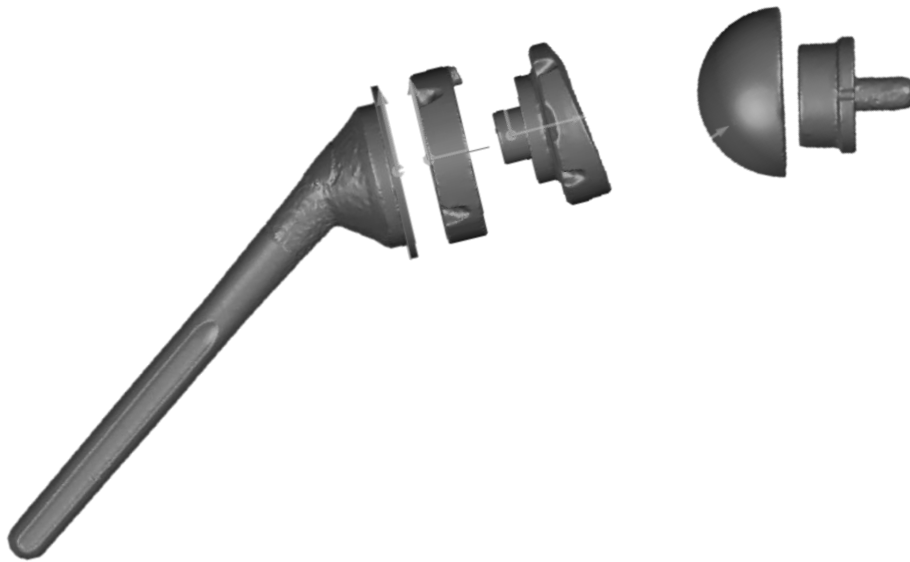
Figure 18. Zimmer's Trabecular Metal RSA system model after laser scanning and applying edits on Geomagic Studio. Basic shapes were fitted to the merged laser scans to improve the accuracy of the parts.

The glenosphere and humeral components were virtually inserted following manufacturer-recommended guidelines and checked by a surgeon (Fig.19) [63]. The glenoid

component baseplate was placed in neutral version with a 2° inferior tilt and was aligned with the

inferior border of the glenoid. The scapular insertion plane was placed in the lateral-most

position allowing for the most scapular bone retention without sacrificing plane uniformity. The

humeral component stem was centrally aligned to the humeral neck while the cup was centrally

aligned to a plane proximal to the anatomical neck (Fig. 19).

Glenoid
component
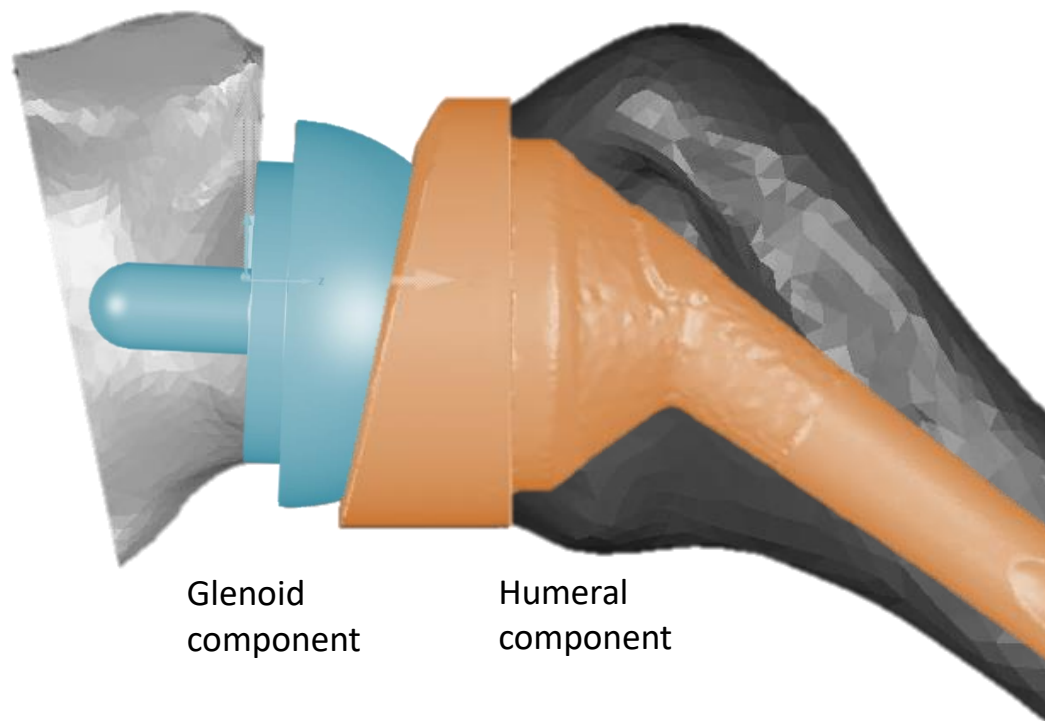
Humeral
component

Figure 19. Whereas the glenoid component of the RSA implant was aligned to the inferior
scapular ridge (left, grey), the humeral component was centrally aligned to the proximal humerus
(right, blue).

The humeral subscapularis insertion point was located adjacent to the lesser tubercle,

while the infraspinatus insertion was located posterior to the greater tubercle [39] (Fig. 20). The

24

insertion site of the lateral section of the deltoid onto the humerus is located on the deltoid tubercle, located more distally than the area covered in the model, which contributed to its position in the model. Due to the supraspinatus being absent in most candidates for RSA, it was excluded from the model.
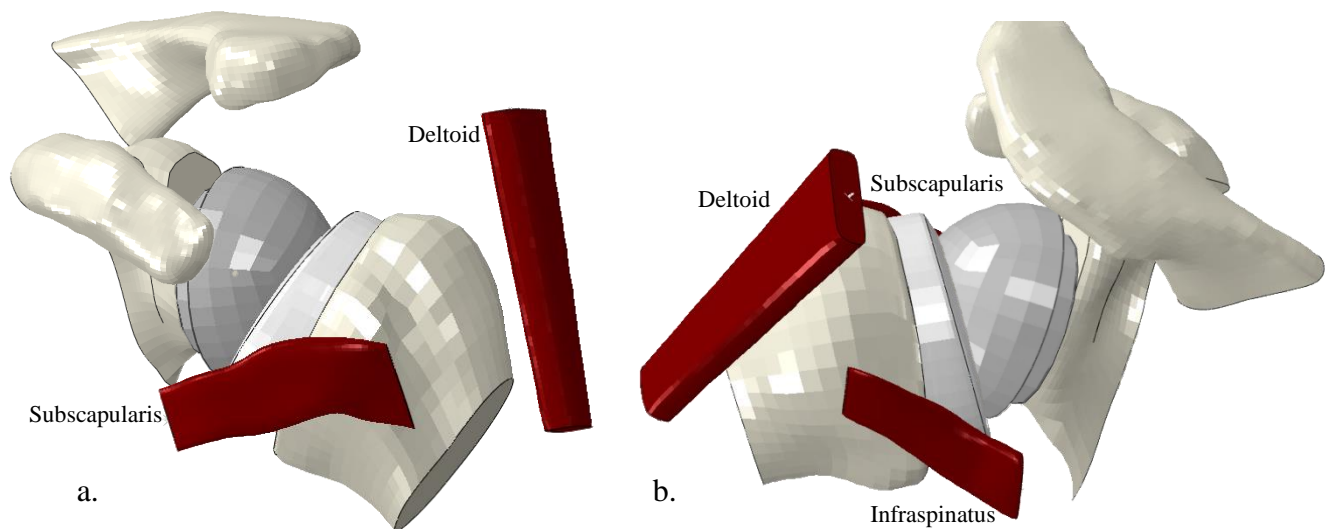
Figure 20. Insertion sites for the subscapularis, infraspinatus, and lateral section of the deltoid on the humeral (distal ends of the soft tissue) were approximated with the aid of an orthopedic surgeon. The proximal ends of all soft tissue were stretched until they reached their anatomical position during testing. Shown above is an anterior view (a), and cranio-posterior oblique view (b) of the RSA-inserted shoulder model. *The insertion site of the deltoid onto the humerus is located on the deltoid tubercle, located more distally than the area covered in the model.

2.3 MESHING

Hexahedral FE meshes were created using TrueGrid parametric preprocessing software (XYZ Scientific) for bones, implant components, and soft tissues. Hexahedral brick elements, composed of 8 vertices and 12 edges, show higher levels of accuracy and efficiency compared to other 3D elements, such as tetrahedral elements, at the cost of being more time consuming [3, 44, 56]. TrueGrid scripting was used to modify glenoid geometry to accommodate different

25

lateralizations. Detailed stereolithography files (ASCII stl files) of the surface geometry were transferred from Geomagic to TrueGrid. Multi-block parts composed of hexahedral elements were then approximated to fit the uploaded surfaces using script parameters and on-screen adjustments. Irregular surface regions were addressed by using the butterfly technique, which involves eliminating a corner block of a part and then gluing the two remaining sides together prior to projecting blocks onto surfaces (Fig. 21). Parts were glued together by using block boundary commands to create continuous meshes throughout the component from several independently created meshes [50].
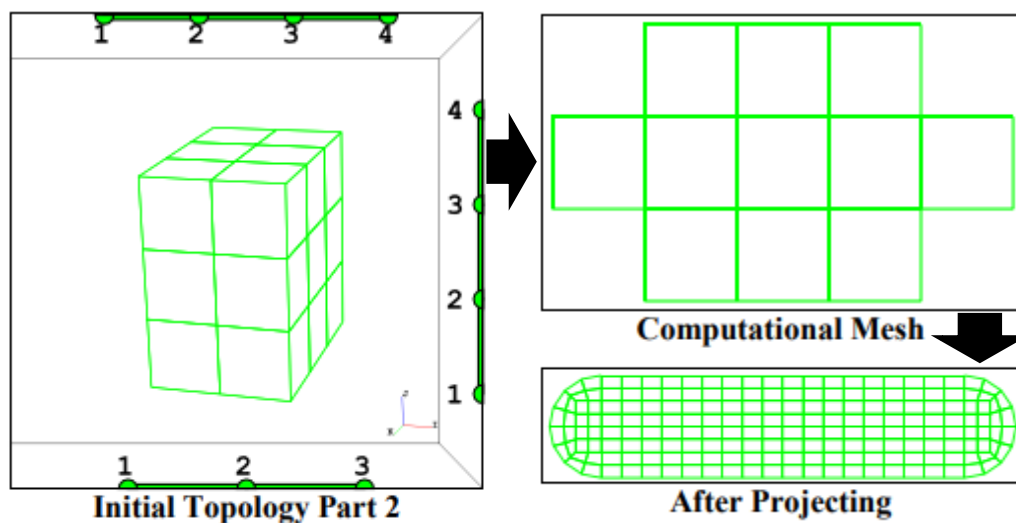
Figure 21. The butterfly mesh technique includes deleting the corners of a block and then gluing the boundaries together to allow the block to adapt to curved surfaces. [42]

TrueGrid Meshes were uniformed and merged (Fig. 22) (Fig. 23) after checking acceptable Jacobian and orthogonality values. Each component was modified to only have positive Jacobian values; negative Jacobian values indicate inverted elements, which prevent FE models from running [30]. Likewise, the angles of the hexahedral mesh were kept within 60° of

orthogonality (90°) to minimize calculation errors and significant deviations at any area while still allowing the mesh to adapt to irregular geometry. Final TrueGrid meshes were exported as Abaqus input files and then formatted to maximize compatibility with Abaqus CAE and user readability.

Glenosphere

Lateralizing Cylinder

Scapula (top)

Scapula (bottom)

Merged glenoid component
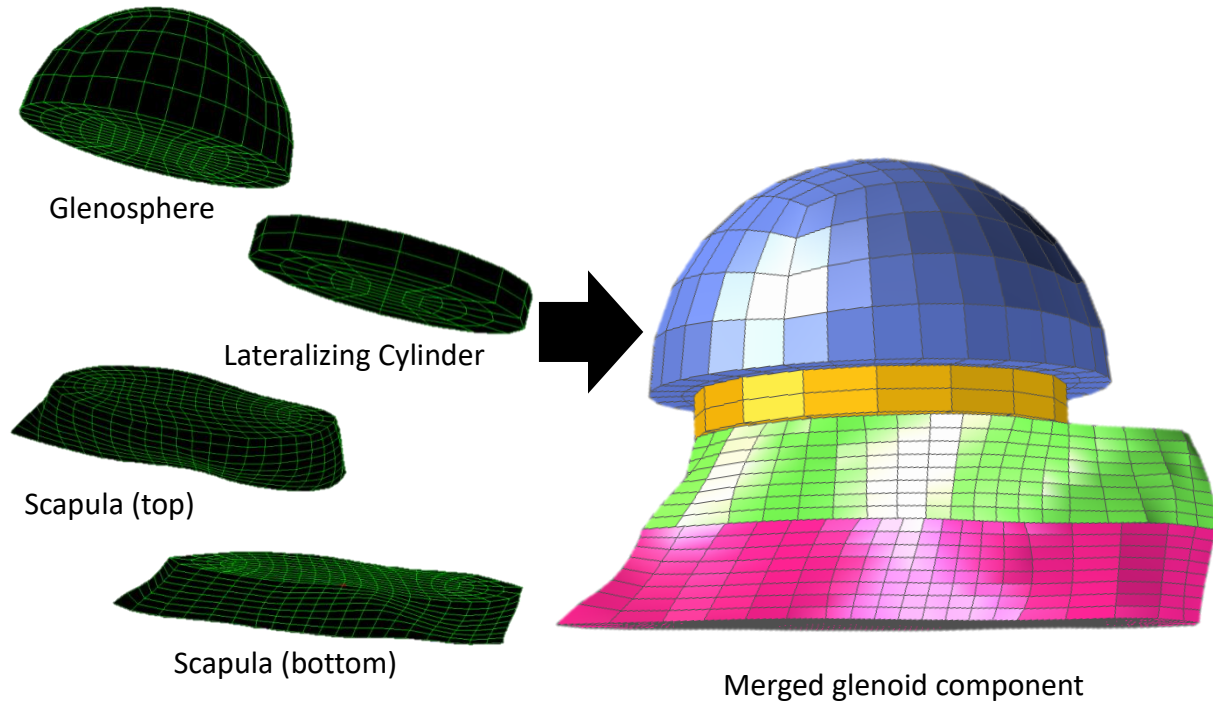
Figure 22. Independently meshed parts created on TrueGrid were merged to create a continuous mesh for the glenoid component shown above. *The acromion and coracoid are not shown for image clarity but were used for all tests.
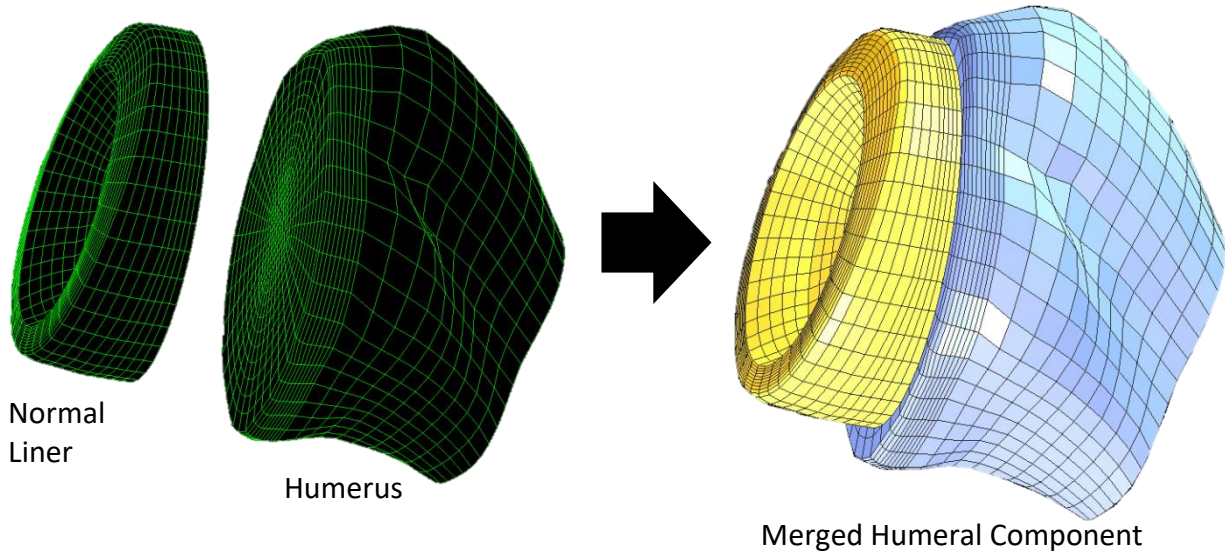
Figure 23. Independently meshed parts created on TrueGrid were merged to create a continuous mesh of the humeral component shown above.

2.4 TESTING

A previously validated FE modeling approach was extended to model shoulder external rotation (ER) after implantation of the Zimmer Trabecular Metal RSA system. The finite element model included a deformable scapula, polyethylene liner, rotator cuff tendons (subscapularis, infraspinatus), and lateral section of the deltoid. Also included were rigid models of the glenosphere, humeral component, and humerus, along with the distal ends of the soft tissue (Fig. 24).
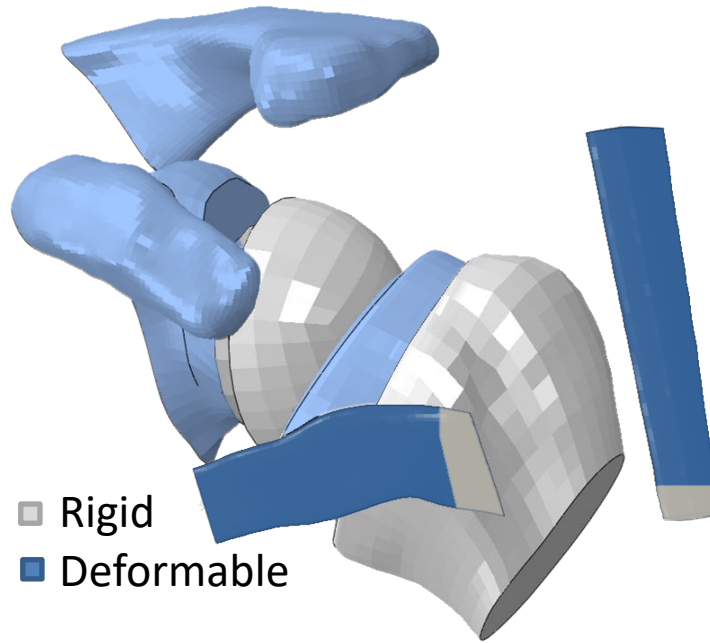
Figure 24. Scapular bone, polyethylene liner, and soft tissues were deformable (blue), while the glenosphere, lateralizing cylinder, humeral bone, and distal ends of the soft tissues were rigid (grey).

Six different models matched glenospheres in three cases of lateralization (2mm, 4mm, and 10mm) with two humeral poly liner designs (normal: 150° neck shaft angle or retentive: 155° neck shaft angle) (Fig. 25). Implant components were fixed to their corresponding bone throughout the motions. The soft tissues were assigned liner elastic material properties using data from prior mechanical testing. They were rigidly fixed to the humerus, while their proximal ends had springs attached to them to guide their motion and to support force development. Proximal springs were located in the center of the proximal end of the soft tissue structures, oriented along the muscle line of action, and assigned stiffnesses of 100N/mm. General contact was assigned, with a friction coefficient set to 0.05. Elastic modulus values for soft tissue were taken from a previous study [46, 47, 48]. Material properties such as Young's modulus, Poisson's ratio, and density can be found in Table 1. For results relating to glenoid lateralization-

29

humeral liner combinations, only the subscapularis and deltoid were used in order to run the

models efficiently. The infraspinatus was used for the model set comparing the effects of

varrying amounts of soft tissue present for the 4mm normal model. The supraspinatus was not

modeled since it is not present for the vast majority of RSA candidates.

Table 1. Material properties for the FE model, included Young's modulus, Poisson's ratio, and density.

Material	Young's Modulus (MPa)	Poisson's ratio	Density (g/cm³)
UHMWPE	500	0.4	0.945
Cortical Bone	15000	0.3	1.8
Subscapularis	130.5	0.45	1.5
Infraspinatus Top	217.45	0.45	1.5
Infraspinatus Bottom	83	0.45	1.5
Deltoid	130.5	0.45	1.5

*4mm lateralized glenoid component shown
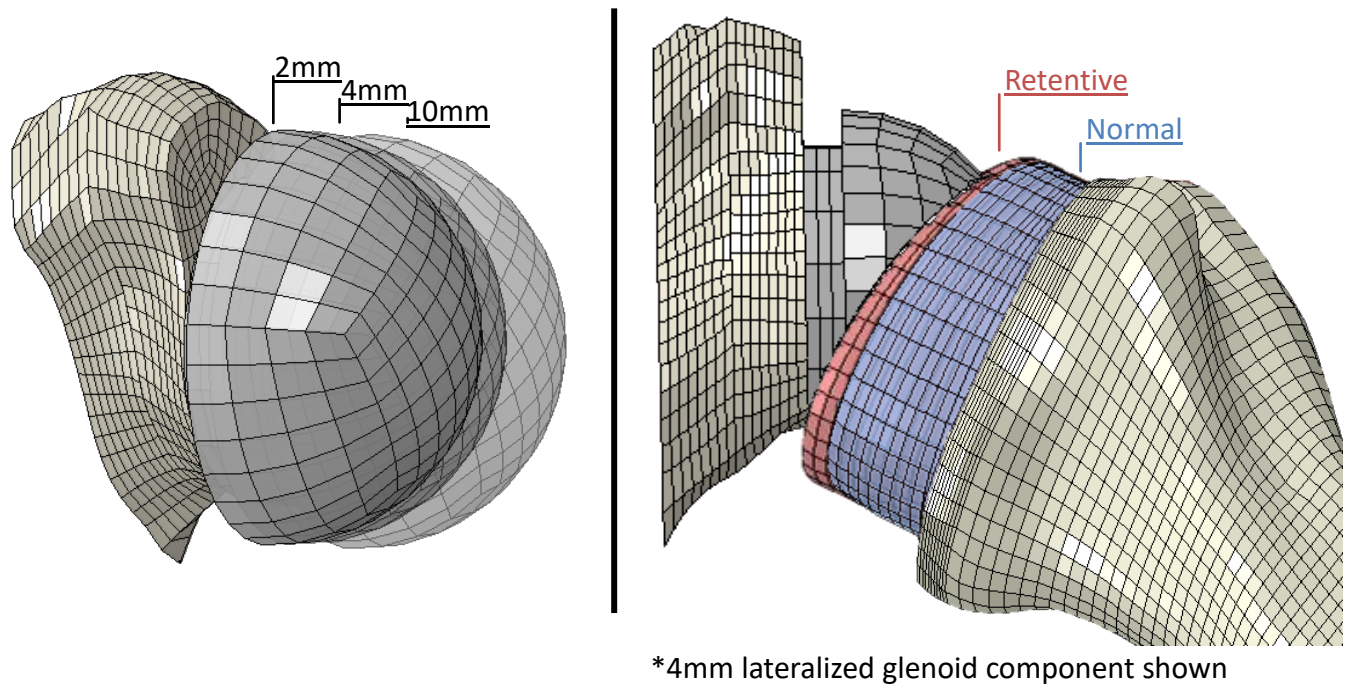
Figure 25. Six different models were created matching three different glenosphere lateralizations (2mm, 4mm, and 10mm) to two humeral liner types (normal and retentive).

The 4mm glenoid lateralization-normal liner model was also used to test inclusion of the tendons and their influence on glenoid component reaction force. Soft tissue testing included the following combinations: deltoid, subscapularis and infraspinatus; deltoid and subscapularis; deltoid and infraspinatus; and deltoid only (Fig. 26). The "deltoid and subscapularis" model in this second part of the study was the same as the "4mm glenoid lateralized, normal humeral liner" model in the first part of the study. Beyond inclusion or exclusion of the muscle groups, all conditions replicated the first part of the study investigating combinations of glenoid component lateralization and humeral liner type.

Figure 26. Four models varying in soft tissue inclusion were created. "Delt Sub Inf" included the deltoid, subscapularis, and infraspinatus; "Delt Sub" included the deltoid and subscapularis; "Delt Inf" included the deltoid and infraspinatus; and "Delt Only" included the deltoid.

The FE analysis was divided into three steps. Throughout the three steps, the scapula (including the acromion and coracoid) was fixed through the glenosphere center of rotation. Also, throughout the run, the distal ends of the soft tissue were tied to the humerus, and each implant component was fixed to its corresponding bone. The first step of the analysis involved pulling the proximal ends of the soft tissues medially and outwardly from the original position. The second step pulled the proximal ends of the soft tissues inwardly toward their anatomical origins. Dividing this process into two steps allowed the tissue to wrap around the implant system and avoid premature contact as tension developed within them (Fig 27). The humeral component and humerus, including the distal ends of the soft tissues that were attached to it, was held fixed through the humeral COR during the first two steps. For the third step, the tensioned proximal ends of the soft tissue were held fixed in space. The humerus was externally rotated at least 80° about the humeral long axis from a neutral position with the shoulder abducted 25° (Fig. 28). This was accomplished by applying a rotational velocity to the humerus (with implanted components) at the center of rotation of the humeral liner around the long axis of the humeral shaft.
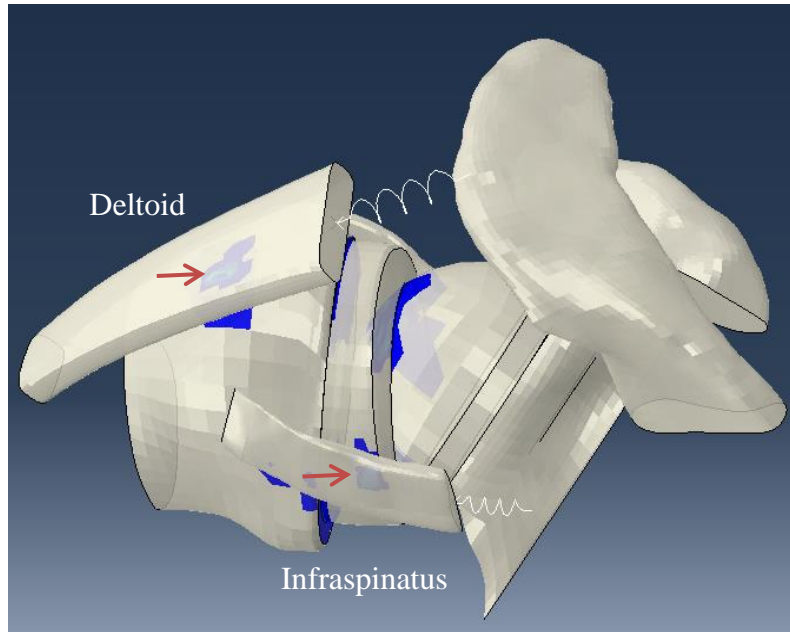
Figure 27. Continuous element representations allowed for contact between the soft tissues and other surfaces (indicated with red arrows) as the soft tissues wrapped around the implant system.

| a. Initial Position | b. After tensioning, before ER motion | c. Final position, after ER motion |
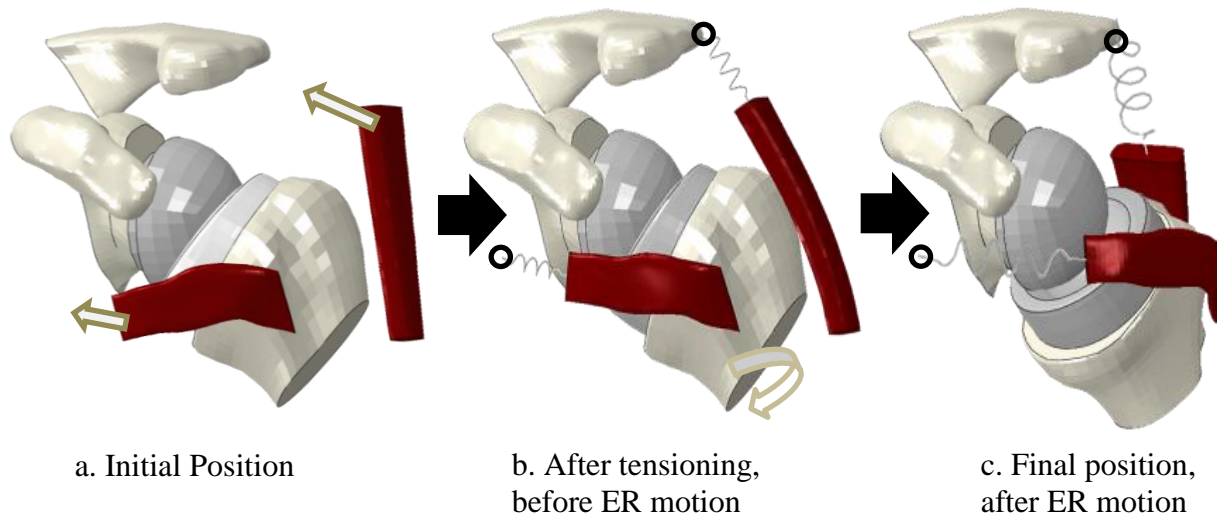
Figure 28. Assembly of the 4mm lateralized glenosphere, normal poly liner model prior to soft tissue tensioning (a), after tensioning immediately before external rotation (b) and final position after external rotation (c). Indicated by the circles, the soft tissues were fixed in space after tensioning.

33

2.5 DATA ANALYSIS

The x, y, z, displacements of the humeral COR, subluxation gap distance, deltoid force, subscapularis force, contact stress, and impingement-free ROM were recorded for models combining varying glenoid lateralization and humeral liner types, as well as for the models differing in muscle inclusion. The subluxation gap distance was defined as the magnitude of x, y, z displacement between the centers of rotation of the poly liner and glenosphere (Fig. 29) and found using the following equation:

$$Total\ Subluxation = \sqrt{x_{disp}^2 + y_{disp}^2 + z_{disp}^2}$$

while the ER angle from the initial position was found using the following equation:

$$ER\ Angle = \sqrt{x_{rot}^2 + y_{rot}^2 + z_{rot}^2}$$

for any value above 0.5mm, a threshold below which relative motions between the articulating parts were deemed as unlikely to be considered clinically relevant.
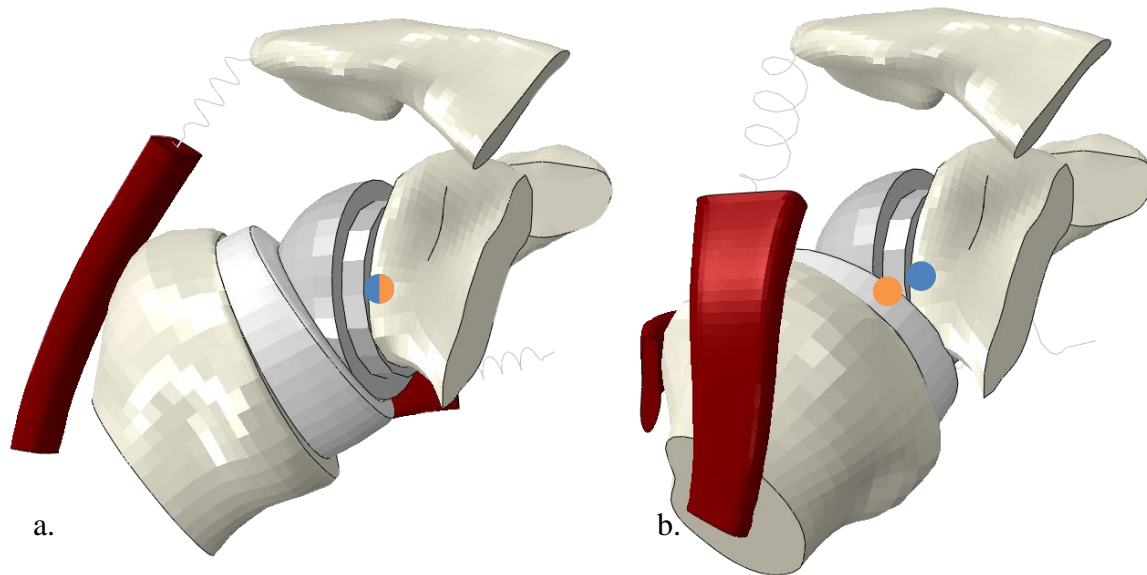
Figure 29. Subluxation was calculated to be the norm of the displacement between the humeral liner COR (orange) to the glenosphere COR (blue). The humeral liner COR coincides with the glenosphere COR from the initial position (a) up until impingement. After impingement, the humeral liner COR diverges from the glenosphere COR (b).

34

CHAPTER 3: RESULTS

3.1 GLENOID LATERALIZATION – POLY LINER COMBINATION RESULTS

Greater impingement-free ROM was observed both for non-retentive liners and with increased glenoid lateralizations (Table 2). For 2mm of lateralization, the normal liner model had 40.5° impingement-free ROM, while the retentive model had 32.4°. The 4mm lateralized models had 48.6° and 36.5° impingement free ROM for normal and retentive liners (respectively). The 10mm models had impingement free ROMs of 68.9° for normal and 60.8° for retentive liners. At 60° of ER motion, the normal, 2mm model displayed 2.9mm of subluxation while the retentive, 2mm model displayed 5.2mm of subluxation. The normal 4mm model displayed 1.8mm of subluxation at 60° of ER motion while the retentive 4mm model had 3.3mm of subluxation. Both 10mm models impinged beyond 60° of external rotation motion, thus no subluxation values were recorded.

Table 2. Impingement-free ROM for external rotation
(subluxation at 60°) for each model.

Lateralization	Normal	Retentive
2mm	40.5° (2.9mm)	32.4° (5.2mm)
4mm	48.6° (1.8mm)	36.5° (3.3mm)
10mm	68.9° (--)	60.8° (--)

After impingement, continued ER motion led to increased subluxation, among all models (Fig. 30). Prior to impingement, dislocation values were negligible (below 0.5mm total). Following RSA, the restoration of glenohumeral ER motion is rarely above 60°, thus this was used as a marker for subluxation comparisons. Retentive liner models impinged earlier than their non-retentive counterparts and because of that had higher subluxation values than non-retentive models at any angle post-impingement. Likewise, models with less glenoid lateralization impinged earlier than did models with greater lateralization. For example, for the models with the same liner category, the 2mm lateralized model impinged before 4mm lateralized model, and 4mm lateralized model impinged before the 10mm model. Models with lower lateralization values also had higher subluxation values than did their counterparts for any ER angle post-impingement. Unlike the 2mm and 4mm models, both 10 mm models impinged after 60°.
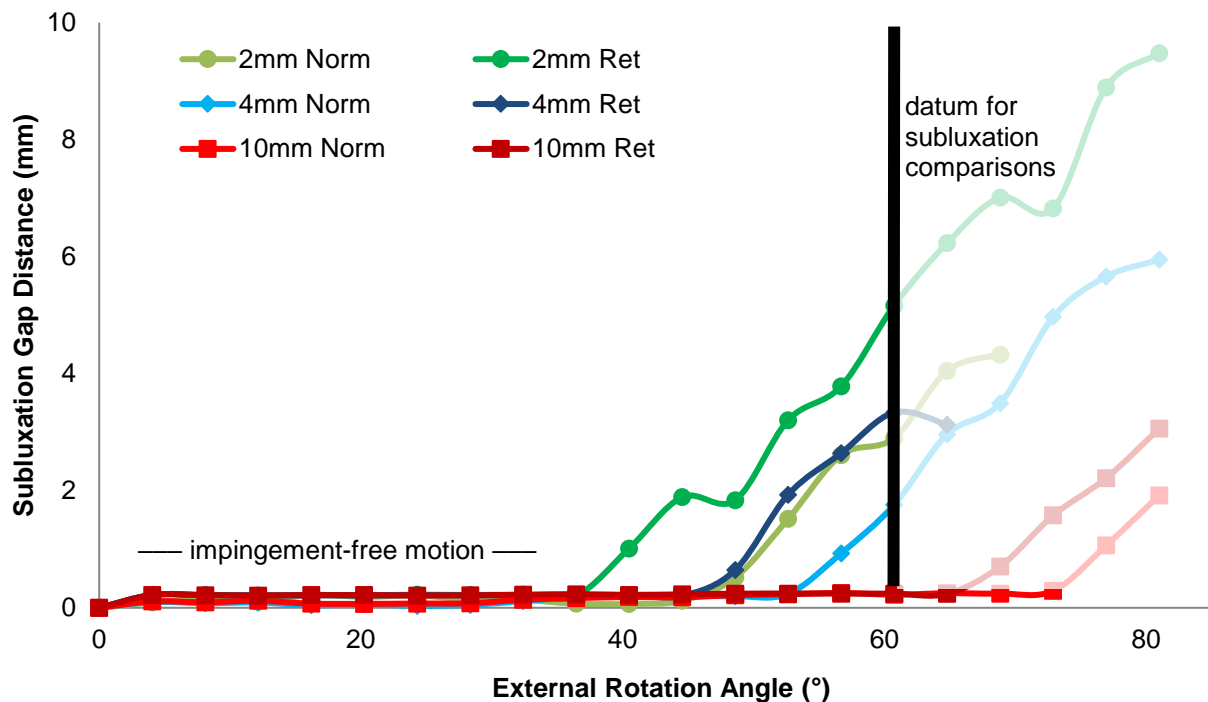
Figure 30. Total subluxation gap distance present through 60° of external rotation from the neutral position for models varying in glenoid lateralization (2mm, 4mm, and 10mm) and poly liner type (retentive (ret) and normal (norm).

36

Initial deltoid and subscapularis tensions were highest for the 10mm models, followed by the 4mm models, and lastly the 2mm models (Fig. 31) (Fig. 32). Initial retentive liner deltoid and subscapularis values were slightly higher than their normal counterparts. In general, greater tensions developed throughout the ER motion for increased lateralizations and for the retentive liners. Post impingement, the 2mm retentive had a higher rate of increasing force for both deltoid and subscapularis tension compared to other models. Lower lateralization values showed more variability in subscapularis forces post-impingement compared to higher lateralization values, with the 10mm models showing the least change in rate of increasing subscapularis force.
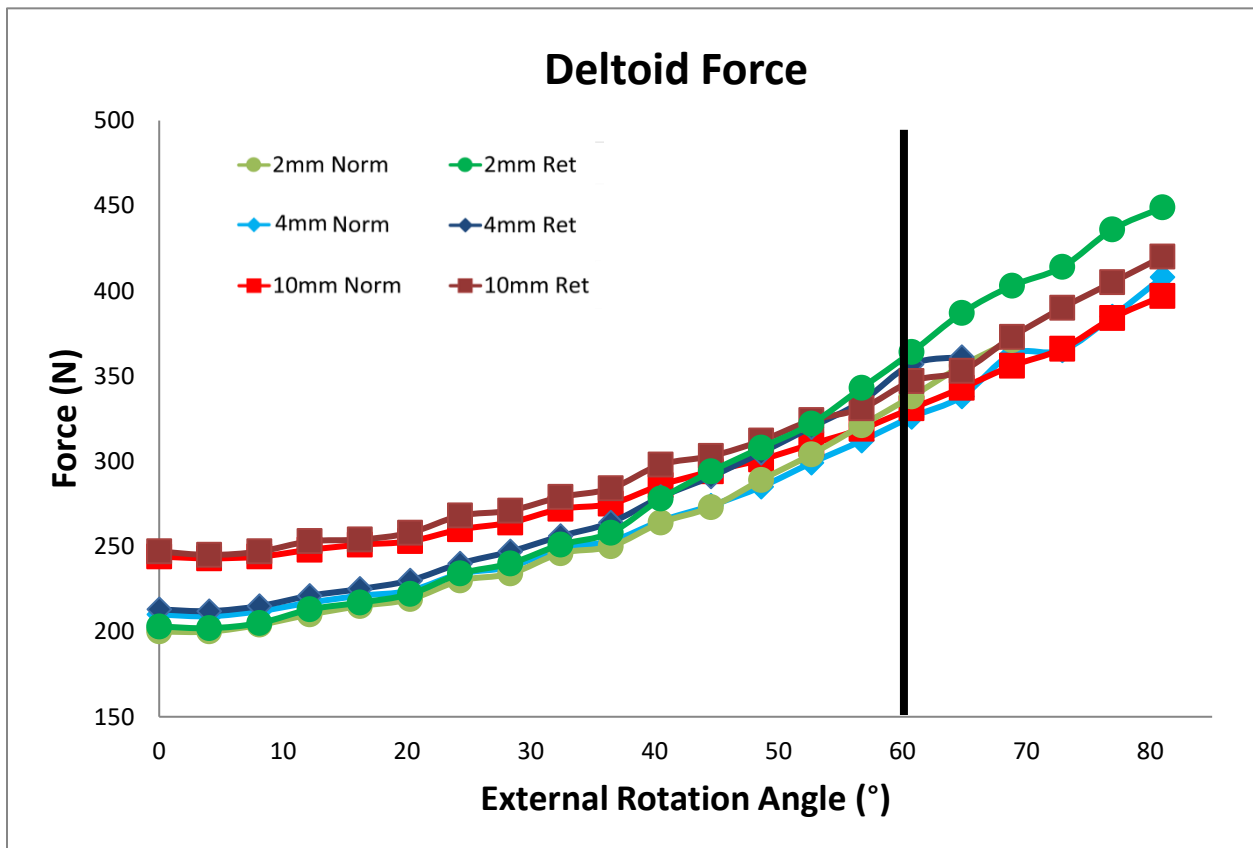
Figure 31. Deltoid force for the six models varying in glenoid lateralization (2mm, 4mm, and 10mm) and poly liner type (retentive (ret) and normal (norm).
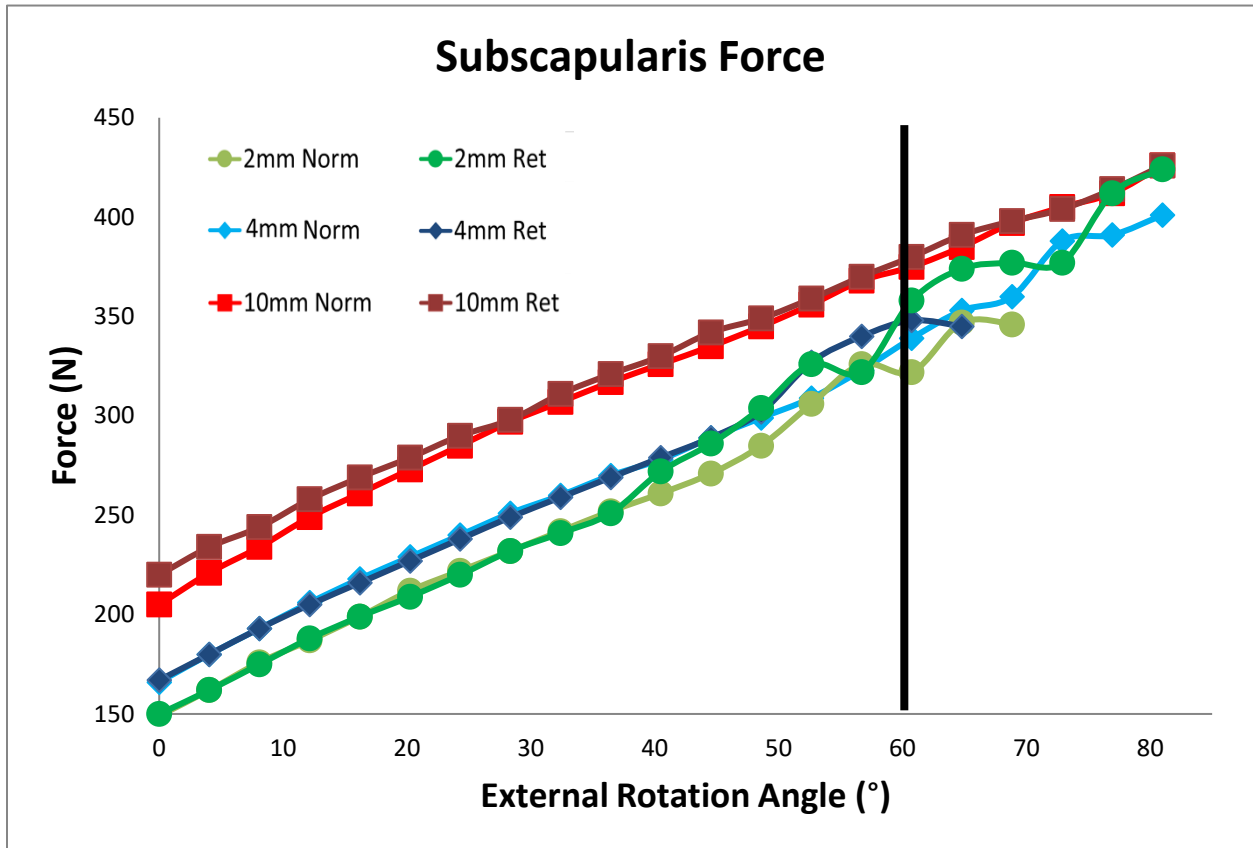
Figure 32. Subscapularis force for models varying in lateralization (2mm, 4mm, and 10mm) and poly liner type (retentive (ret) and normal (norm)).

Models with higher glenoid lateralizations had increasingly lateral impingement sites on the scapula, with the impingement for 10mm lateralized baseplate-retentive liner combination being most lateral (Fig. 33). Retentive and normal liners appeared to impinge in the same general area in the inferior scapula (Fig. 34).

38
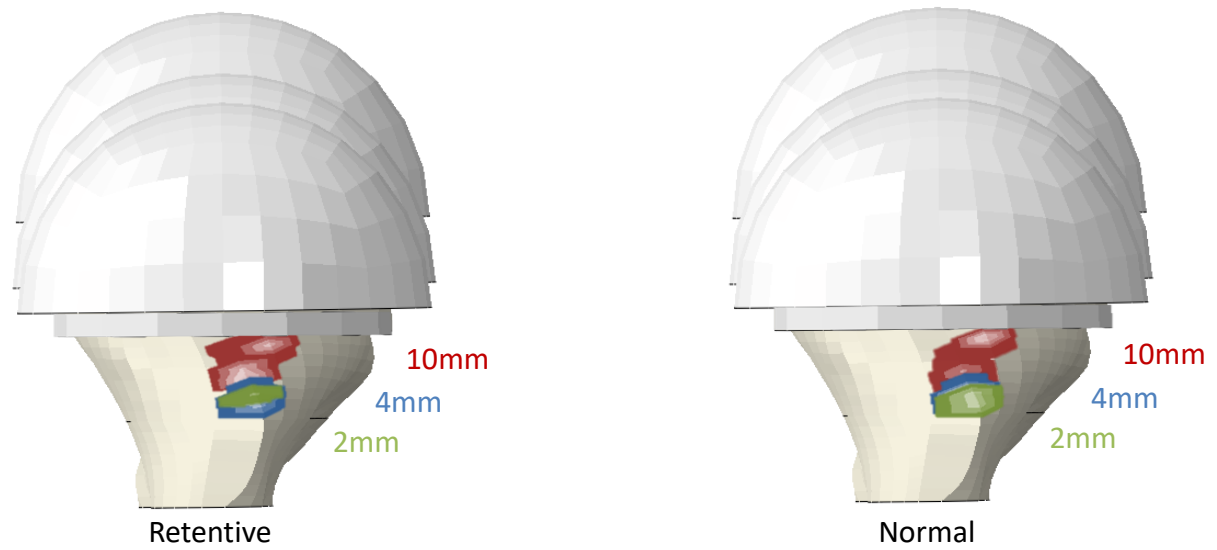
Figure 33. Comparison of initial contact stress on the inferior scapular at 2mm (green), 4mm (blue) and 10mm (red) glenoid lateralizations for retentive and non-retentive humeral liners.
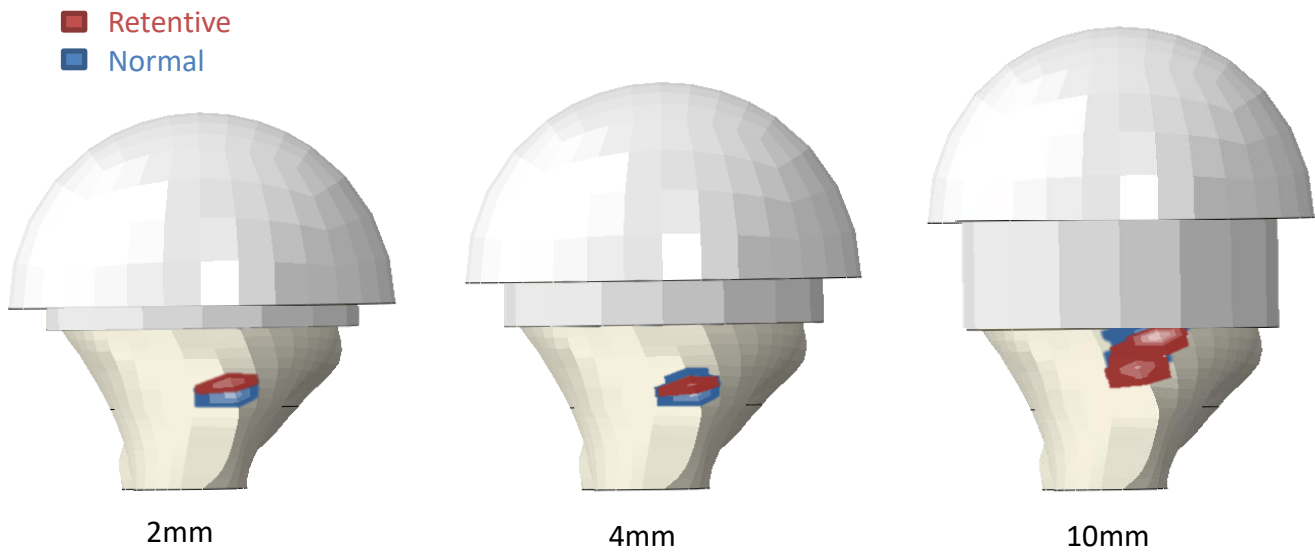
Figure 34. Comparison of initial contact stress on the inferior scapular for retentive (red) and non-retentive (blue) humeral liners for different lateralization values (2mm, 4mm, and 10mm).

Subluxations for most models tended to follow increasingly inferior, anterior, medial paths, with the exception of the 2mm retentive model, which moved posteriorly instead of anteriorly (Fig. 35) (Fig. 36) (Fig. 37). Dislocation values started to increment and spread from the original location once each of the models impinged with the glenoid bone. The 2mm retentive model had the highest amount of lateral, superior, and posterior dislocation compared to the other models at 60° of ER motion. Alternatively, the 4mm retentive model had the highest amounts of medial, inferior, and anterior displacement at 60° of ER motion compared to the other models at that angle.
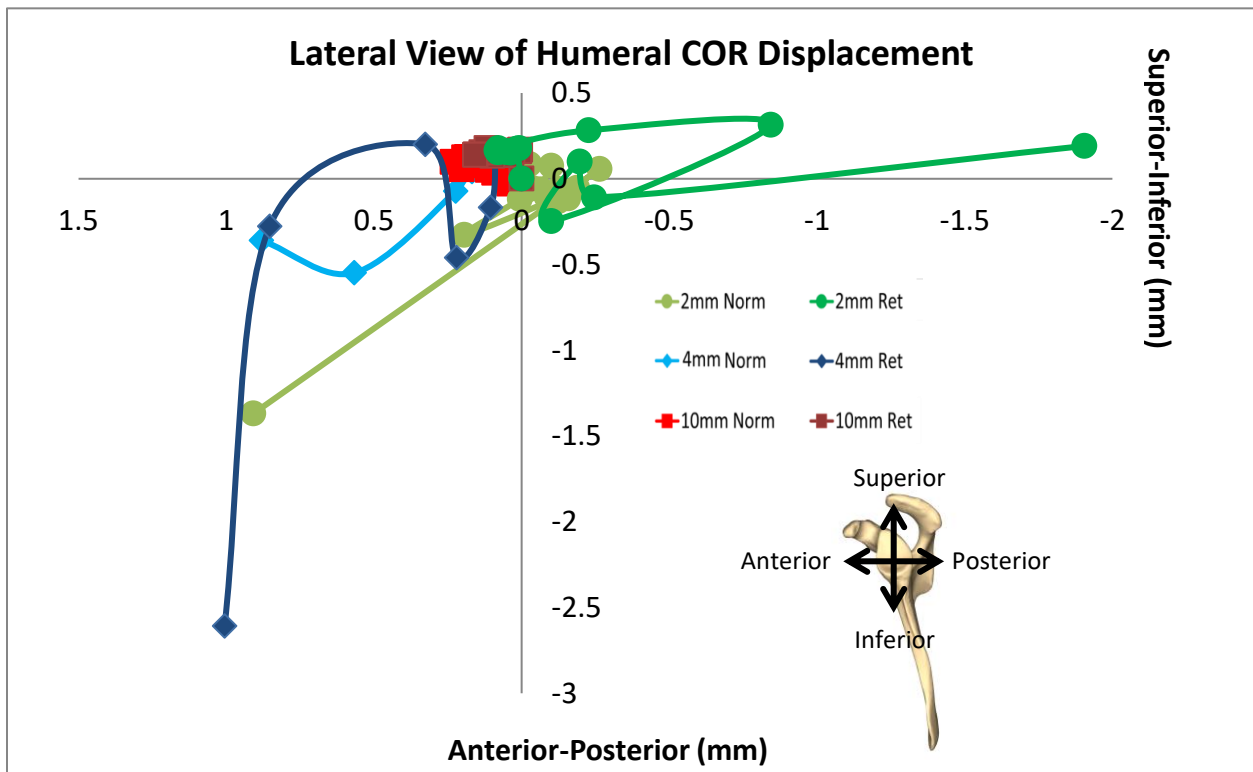
Figure 35. Lateral view of the shoulder showing humeral COR anterior-posterior and superior-inferior displacement until 60° of ER motion for the six models varying in glenoid lateralization (2mm, 4mm, and 10mm) and poly liner type (retentive (ret) and normal (norm))..
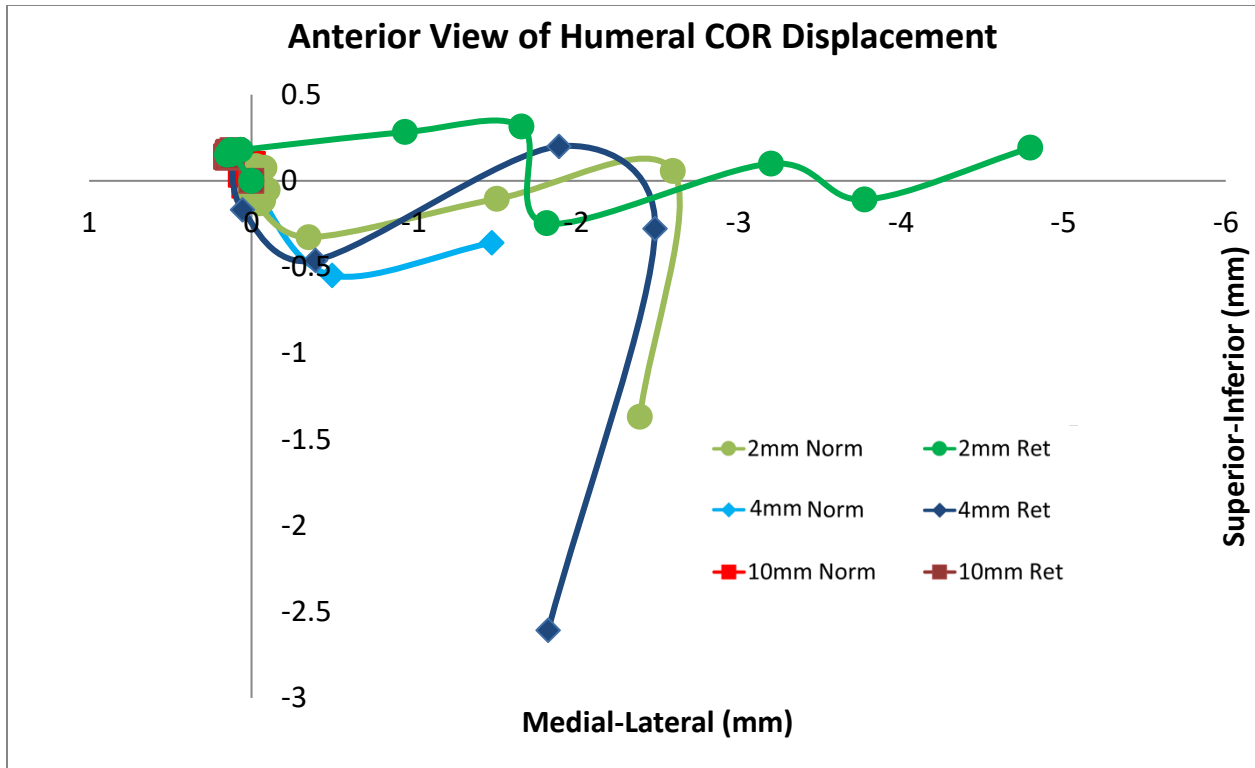
Figure 36. Anterior view of the shoulder showing humeral COR medio-lateral and superior-inferior displacement until 60° of ER motion for the six models varying in glenoid lateralization (2mm, 4mm, and 10mm) and poly liner type (retentive (ret) and normal (norm).
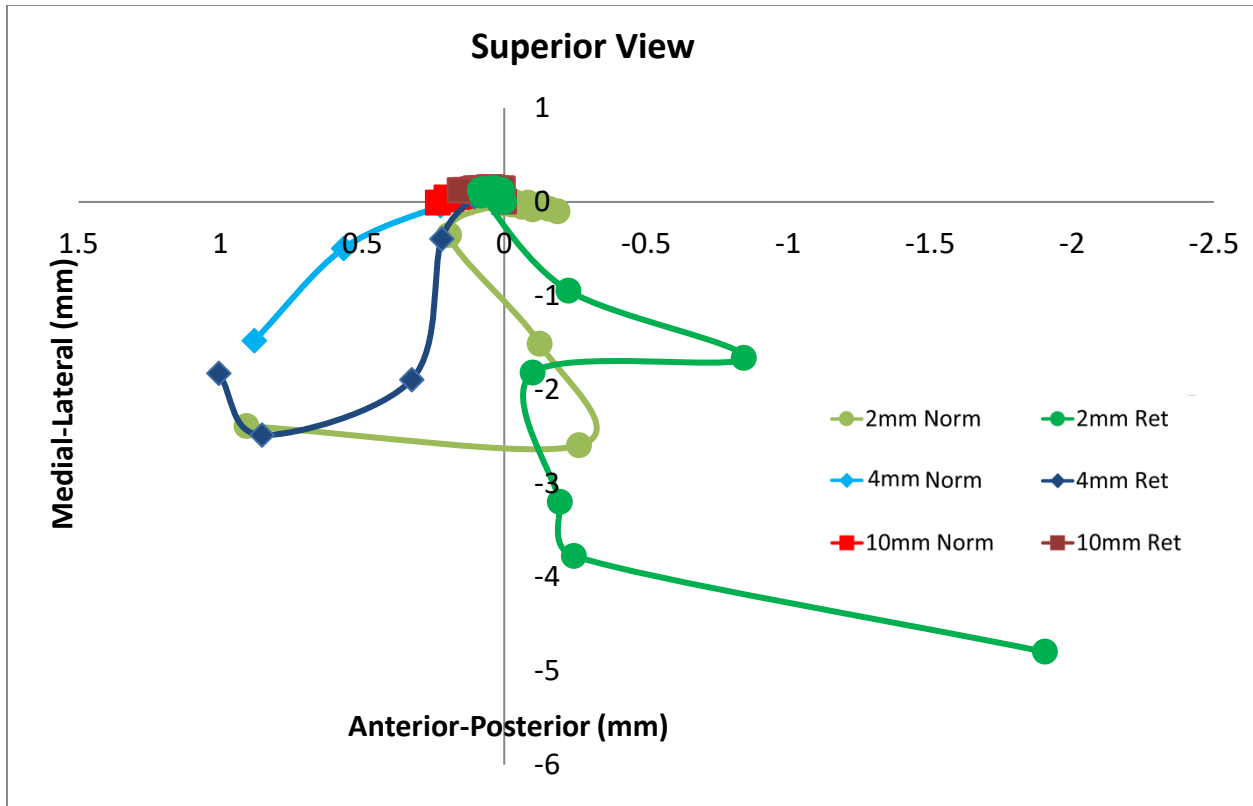
Figure 37. Superior view of the shoulder showing humeral COR anterior-posterior and medial-lateral displacement until 60° of ER motion for the six models varying in glenoid lateralization (2mm, 4mm, and 10mm) and poly liner type (retentive (ret) and normal (norm))..

Maximum contact stress was highest in the 2mm retentive liner (105 MPa), followed by the 2mm normal model (91 MPa), 4mm retentive model (77 MPa), and lastly the 4mm normal model (55 MPa) for ER motion until 60° (Table 3). The 10mm models did not impinge until after 60° of ER, so they were not included. Contact stress values varied but followed generally increasing trends post impingement between the humeral liner and inferior scapula (Fig. 38).

Table 3. Maximum post-impingement contact stress for ER motion up to 60° on the inferior scapula for the six models (angle of maximum contact stress). *The 10mm models impinged above 60° and were thus excluded.

Lateralization	Normal	Retentive
2mm	91 MPa (40.5°)	105 MPa (57°)
4mm	55 MPa (60°)	77 MPa (53°)
10mm	(--)*	(--)*
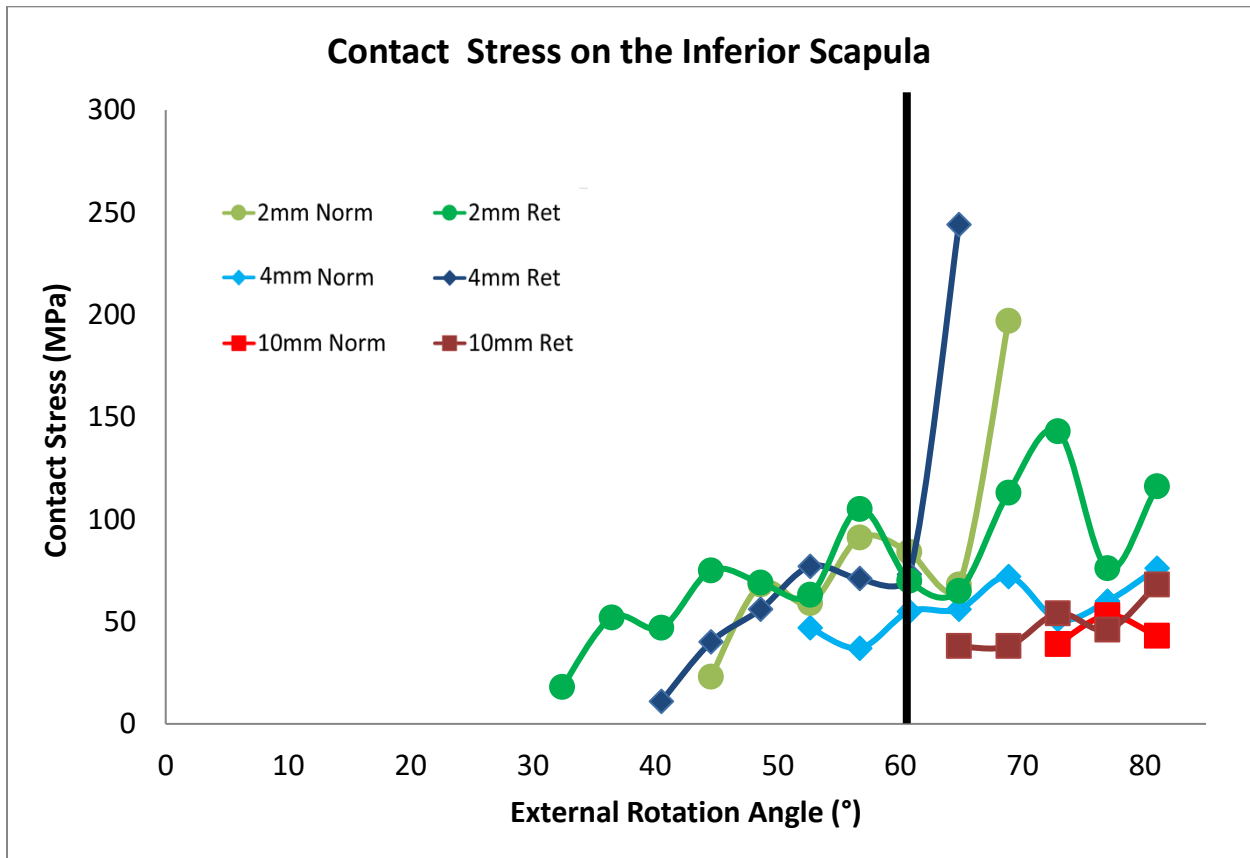
Figure 38. Contact stress value for models varying in combinations of glenoid component lateralization (2mm, 4mm, and 10mm) and poly liner type (retentive (ret) and normal (norm).

3.2 SOFT TISSUE INCLUSION/EXCLUSION RESULTS

As expected, absence of the subscapularis was associated with lower overall reaction forces than for models containing the subscapularis (Fig. 39). Glenoid component reaction forces became more variable as models progressed throughout the ER motion. The model that only included the deltoid had the lowest amount of glenoid reaction force on average prior to impingement and had the most variable post-impingement glenoid component reaction force. All models impinged at 52.7° of external rotation, with 48.6° of impingement free range or motion.
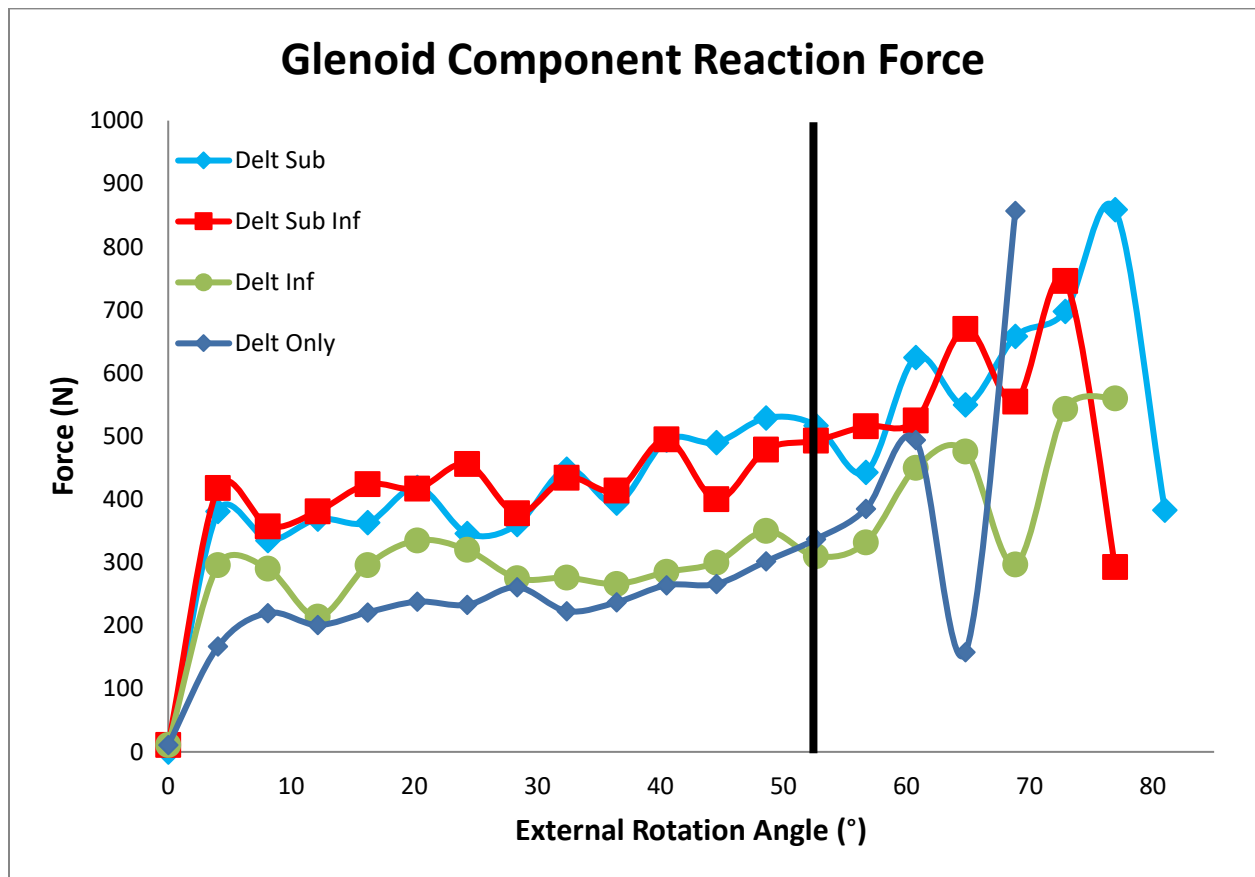
Figure 39. Glenoid reaction forces for 4mm lateralized, non-retentive humeral liner models varying in soft tissue present. "Delt Sub Inf" included the deltoid, subscapularis, and infraspinatus; "Delt Sub" included the deltoid and subscapularis; "Delt Inf" included the deltoid and infraspinatus; and "Delt Only" included the deltoid. *The black marker denotes the angle of initial impingement which was the same for all four models.

Consistently lower subscapularis forces were seen when the infraspinatus was included in the model (Fig. 40). There were no notable differences in the deltoid reaction force for the four models varying in muscle quantities, although all models showed a positive trend between external rotation and deltoid force (Fig. 41).
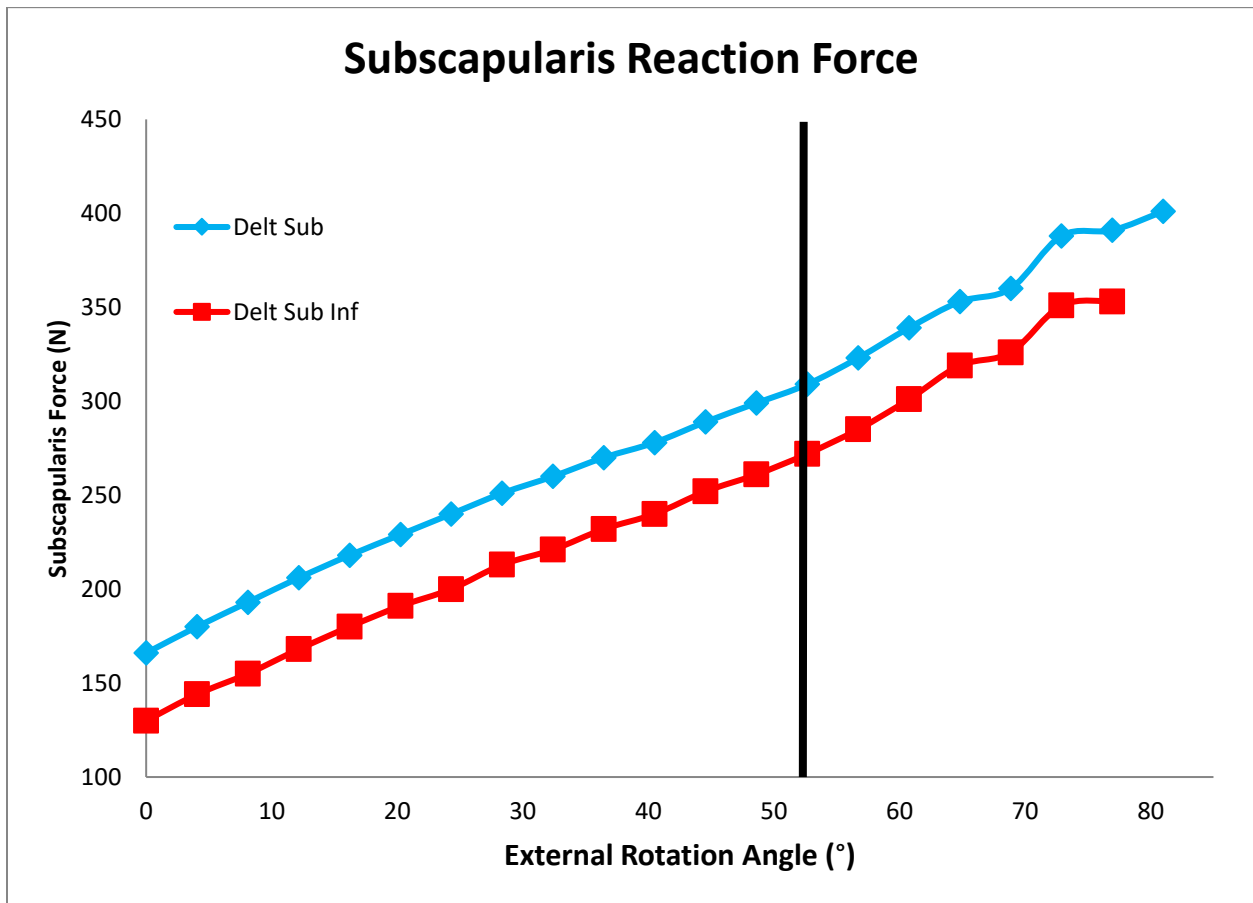
Figure 40. Subscapularis reaction forces for 4mm lateralized, non-retentive humeral liner models varying in soft tissue present. "Delt Sub Inf" included the deltoid, subscapularis, and infraspinatus; "Delt Sub" included the deltoid and subscapularis; "Delt Inf" included the deltoid and infraspinatus; and "Delt Only" included the deltoid. *The black marker denotes the angle of initial impingement which was the same for all four models.
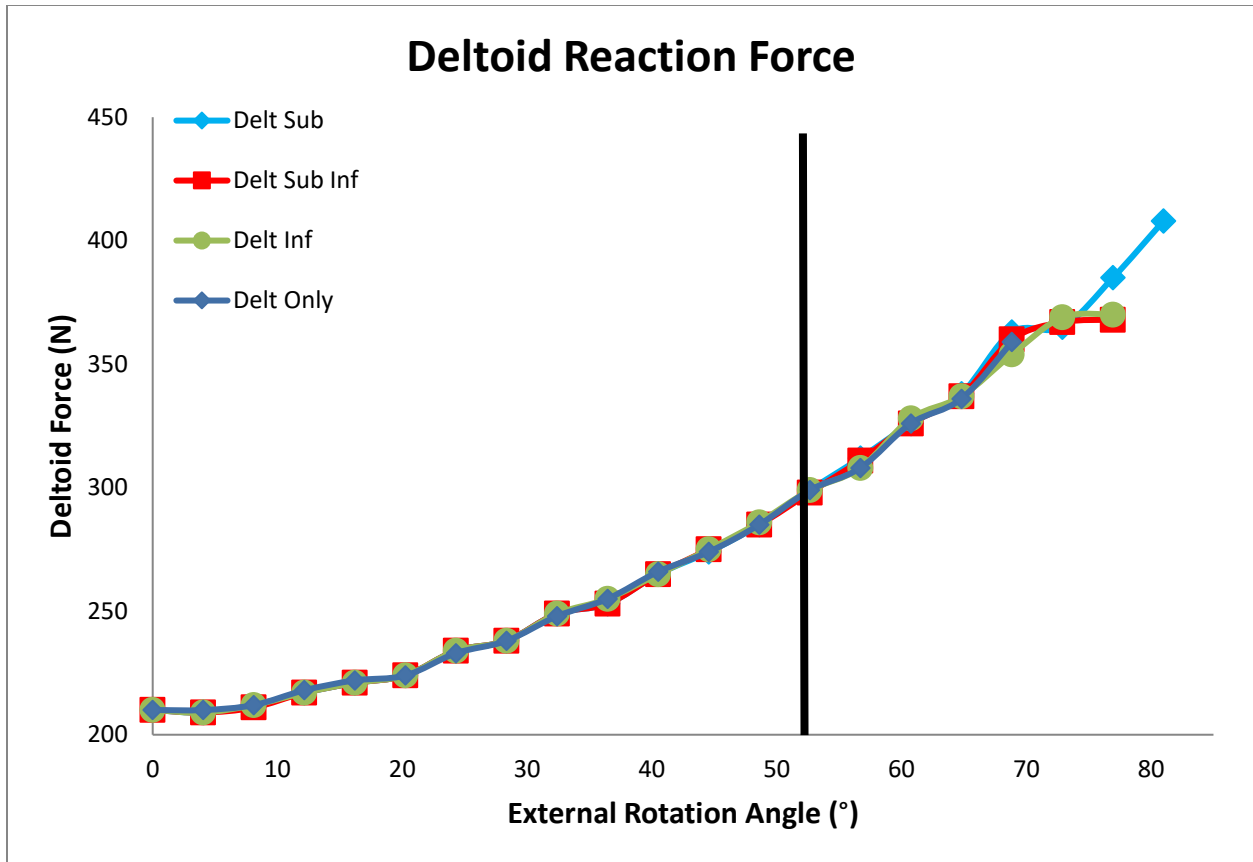
Figure 41. Deltoid Reaction Force for a 4mm lateralized, non-retentive humeral liner model varying in soft tissue present. "Delt Sub Inf" included the deltoid, subscapularis, and infraspinatus; "Delt Sub" included the deltoid and subscapularis; "Delt Inf" included the deltoid and infraspinatus; and "Delt Only" included the deltoid. *The black marker denotes the angle of initial impingement which was the same for all four models.

Contact stress highly varied depending on the combination of musculature included (Fig. 42). Overall contact stress values ranged from the minimum of 2MPa at 68.9° by the "Deltoid

Only" model, to a maximum of 76 MPa at 80° by the "Delt Sub model" throughout the entire run time. All models impinged at the same degree of ER.
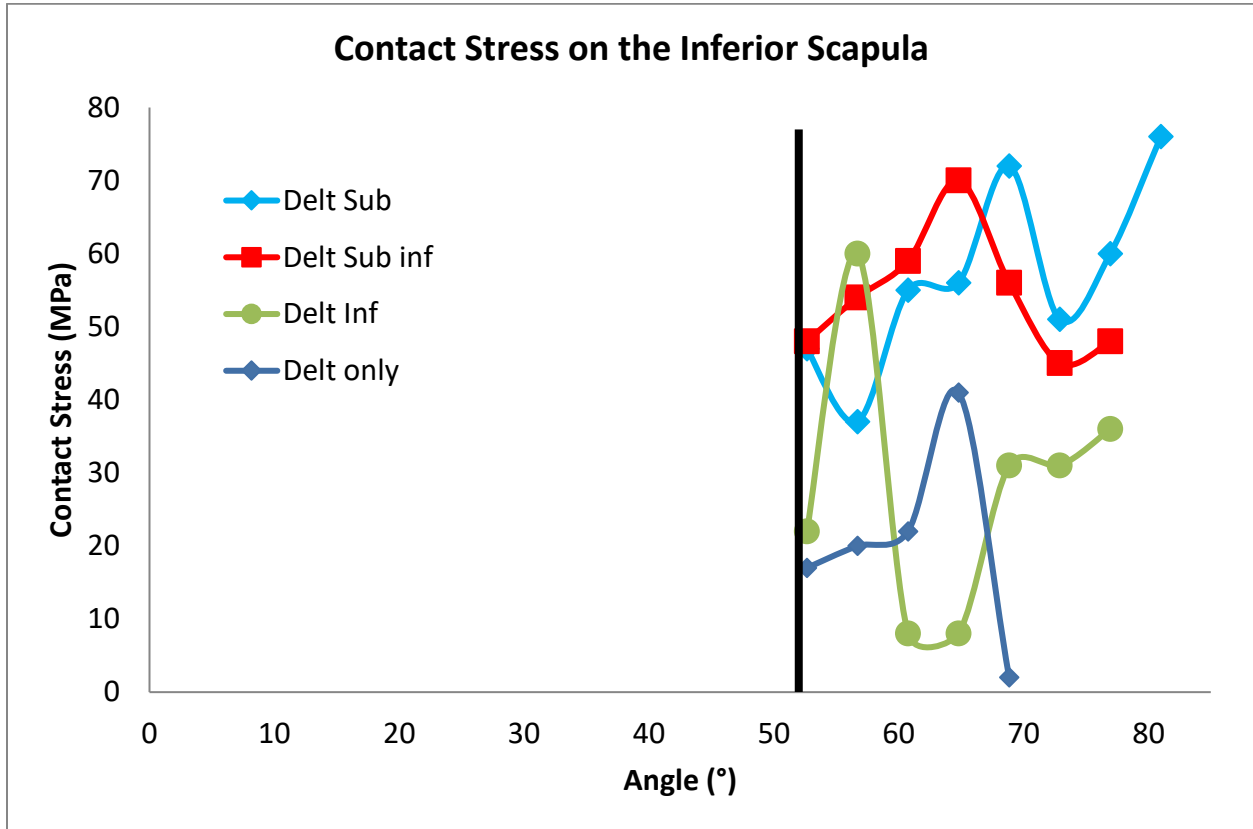
Figure 42. Contact stress on the inferior scapula for 4mm lateralized, normal humeral liner models differing in musculature present up until 60° of external motion. "Delt Sub Inf" included the deltoid, subscapularis, and infraspinatus; "Delt Sub" included the deltoid and subscapularis; "Delt Inf" included the deltoid and infraspinatus; and "Delt Only" included the deltoid. *The black marker denotes the angle of initial impingement which was the same for all four models.

Post-impingement dislocation for all musculature models was in a generally anterior-inferior direction (Fig. 43). Models without a subscapularis tended to move more inferiorly as well as move more irregularly ("Delt Inf and Delt Only"), while models with a subscapularis ("Delt Sub Inf" and "Delt Sub") had more consistent paths.
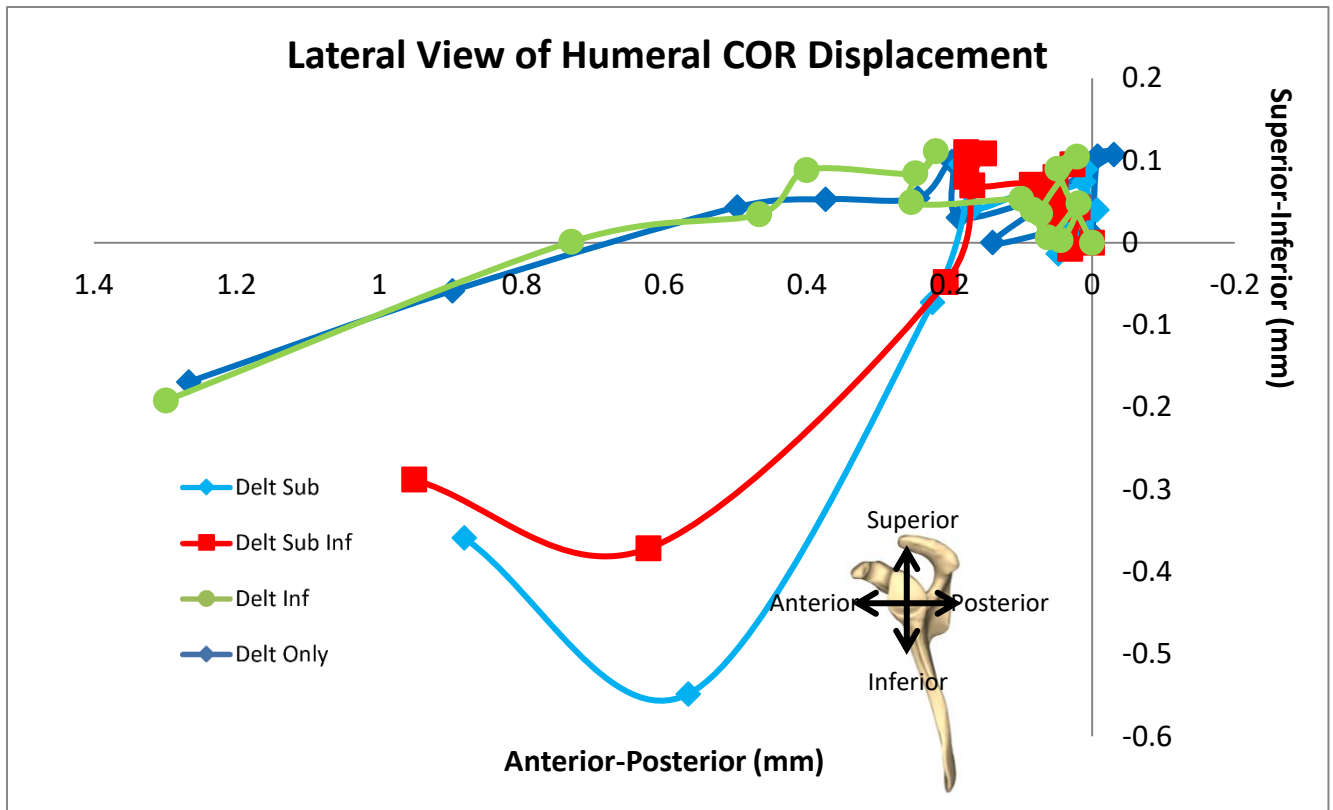
Figure 43. Lateral view of humeral COR displacement for 4mm lateralized, normal humeral liner models differing in musculature present up until 60° of external rotation motion. "Delt Sub Inf" included the deltoid, subscapularis, and infraspinatus; "Delt Sub" included the deltoid and subscapularis; "Delt Inf" included the deltoid and infraspinatus; and "Delt Only" included the deltoid.

CHAPTER 4: DISCUSSION

Instability is one of the most prevalent complications post RSA, yet there are limited studies able to successfully model it post-impingement. Although finite element analysis has been used widely to study the glenohumeral joint of the native shoulder, few studies have been performed to evaluate the shoulder biomechanics post-RSA implantation. Most efforts to model the shoulder post-RSA have used static FE conditions, and simple representations of the soft tissues as pulleys or springs. Dynamic FE models have usually stopped at impingement, neglecting subluxation and other post-impingement behavior that may prove insightful when weighing RSA options during surgical planning. This study used FE analysis to investigate how variations in implant geometry such as lateralization and humeral liner affect shoulder stability following RSA. Instability was also tested by studying the effects of musculature group inclusion.

Although greater glenosphere lateralization was associated with greater impingement-free ROM, it was at the expense of larger deltoid and subscapularis forces. Retentive liners may improve stability, but it comes at the cost of decreased impingement-free ROM and higher soft tissue tensions than the normal liners. Deltoid tension contributes to shoulder stability and control, but elevated amounts of deltoid tension may contribute to scapular fractures and greater stress at impingement sites post-RSA. Both the deltoid and subscapularis force graphs showed elevated initial force values for higher glenoid lateralizations, which mirror the passive tension that would be present post RSA insertion for patients.

The local details of scapular geometry influenced subluxation magnitude and direction, most notably in the 2mm retentive model, which ended up sliding on the posterior side of the inferior scapular ridge instead of the anterior side that all other models followed. The proceeding,

49

diverging path was not only influenced by where and how the poly liner contacted the inferior scapula. The effects of the bony geometry could also be visibly observed watching the dynamic models run past impingement, and volley between subluxation and elevated forces.

Muscle integrity (whether included or not) also influenced the initial point of contact between the humeral liner and scapula, as well as dislocation paths post-impingement. Presence of more soft tissue was associated with greater overall stability. Specifically, presence of the subscapularis seemed to stabilize the shoulder during ER. Elevated contact stresses were found in models that included the subscapularis, but also displayed less variability in dislocation paths. This would indicate more concentrated amounts of force in these areas. Although less than ideal, this would need to be leveraged with the more severe alternative of having unstable, highly variable displacement paths that would scrape along the inferior scapular ridge. Lower subscapularis forces were found in muscle models with higher quantities of muscle groups. This can be attributed to having a wider distribution of the forces between the multiple muscle groups. Whereas the subscapularis seemed to be affected by the amount of additional musculature, the deltoid force was minimally impacted by additional muscle groups. This may be dependent on the motion in question. The lateral deltoid played a stabilizing role in this study, but it is not the primary antagonist for external motion; the subscapularis is.

There were several limitations to this study. Soft tissues were assumed to have linear elastic properties. In real life there would be plateauing of stress values, and an ultimate tensile load that would indicate the upper limits of the muscle's ability to carry load. Pain isn't able to be incorporated in this type of modeling, but would also affect both the trajectory of displacement, and the overall ROM that a patient can handle. The muscles also could not exhibit compressibility, which would affect the behavior of the infraspinatus during external motion.

50

Currently only the lateral section of the deltoid was included, but adding the anterior and posterior portion of the deltoid would allow insight especially during anterior and posterior motion. Muscles are also composed of highly variable distributions of different types of fiber which would affect the literature values for mechanical properties of a certain area. For example, the length-tension relationship is affected by the size and shape of a muscle specimen (specifically the thickness of the specimen) along with testing specifications such as stretching a piece of musculature along verses perpendicularly to the lines of action.

Further analysis incorporating greater anatomical fidelity and modeling additional motions may offer greater insight to orthopedic surgeons when planning for RSA insertion. Testing abduction motion may be of particular interest now that the coracoid, acromion, and deltoid have been incorporated into the model. Retentive liners are marketed as providing additional stability, which the higher forces in this study would support to an extent, but this stability must be weighed against the possibility of limiting patient ROM. Although the subscapularis, infraspinatus, and deltoid were included in the model, the addition of other stabilizing cuff tissues such as the teres minor may be able to not only elevate the accuracy of the model but be able to represent the variety of cuff deficiency found in candidates for RSA. Pairing the finite element analysis to a dynamic musculoskeletal model, or other approaches may also expand the analysis.

Comparison of other combinations of geometrical features of the RSA system, implant insertion sites, and existing patient anatomy may reveal strategies to improve patient outcomes, as well as directly impact choices taken by orthopedic surgeons both before and during RSA implantation. For example, combining a retentive humeral liner with a centralized glenoid placement would increase the risk of scapular notching between the polymer liner and any

51

glenoid bone inferior to the glenoid component placement. Alternatively, glenoid component placement flush with the inferior scapular ridge, or an overhanging placement would decrease scapular notching and scapular impingement, but insufficient bone stock may affect results.

Instability is one of the most common complications found in RSA, yet there is a scarcity of finite element models that are able to capture this phenomenon post-impingement. RSA implant design variations and their effects on patient biomechanics remain an ongoing area of study, especially when multiple design variations are combined. Differing cuff deficiency in patients with RSA also creates an added area that needs to be study. This study focused on how different combinations of glenoid lateralization and humeral liner type affected patient instability, impingement-free ROM, and tension on the lateral deltoid and subscapularis. While greater lateralization of the glenophere increased impingement-free ROM, more tension was created at the deltoid. Retentive liners were associated with lower ROM and greater deltoid forces than their normal counterparts. Smaller impingement-free ROMs were associated with earlier and greater quantities of instability. The subscapularis appeared to have the greatest impact on subluxation and reaction forces compared to other soft tissues. Scapular geometry was also found to influence subluxation paths on the inferior scapula. This study emphasized that both patient anatomy and implant geometry work in tandem to influence outcomes of RSA. The added complexity of this model not only allows more variables related to RSA to be investigated, but also creates a more accurate representation of patient anatomical conditions.

52

REFERENCES

1. Ackland DC, Patel M, Knox D. Prosthesis design and placement in reverse total shoulder arthroplasty. *J Orthop Surg Res*. 2015 Jul 2; 10:101.

2. Aizawa J, Masuda T, Koyama T, Nakamaru K, Isozaki K, Okawa A, Morita S. Three-dimensional motion of the upper extremity joints during various activities of daily living. *Journal of Biomechanics*. 2010; 43:2915–2922.

3. Baker TJ. Mesh generation: Art or science?. *Progress in Aerospace Sciences.* 2005; 41(1):29-63.

4. Bohsali KI, Wirth MA. Reverse Shoulder Arthroplasty: Evolution in Design, Indications, Surgical Technique, and Associated Complications. Gumina S. (eds) *Rotator Cuff Tear*. Springer, Cham; 2017; 391-413.

5. Boileau P, Moineau G, Roussanne Y, O'Shea K. Bony increased-offset reversed shoulder arthroplasty: minimizing scapular impingement while maximizing glenoid fixation. *Clin Orthop Relat Res.* 2011; 469:2558-2567. 10.1007/s11999-011-1775-4.

6. Boileau P, Sinnerton RJ, Chuinard C, Walch G. Arthroplasty of the shoulder. *The Journal of Bone and Joint Surgery British Volume.* 2006; 88:562-575.

7. Boileau P, Watkinson D, Hatzidakis AM, Hovorka I. Neer Award 2005: The Grammont reverse shoulder prosthesis: results in cuff tear arthritis, fracture sequelae, and revision arthroplasty. *J Shoulder Elbow Surg.* 2006; 15:527-540.

8. Boileau P, Watkinson DJ, Hatzidakis AM, Balg F. Grammont reverse prosthesis: design, rationale, and biomechanics. *J Shoulder Elbow Surg.* 2005;

9. Boileau P. Complications and revision of reverse total shoulder arthroplasty. *OTSR*. 2016; 102:S33-43.

10. Boileau P, Melis B, Duperron D, Moineau G, Rumian AP, Han Y. *J Shoulder Elbow Surg.* 2013; 22(10):1359-1370.

11. Brand RA, Mont MA, Manring MM. Biographical sketch: Themistocles Gluck (1853-1942). *Clin Orthop Relat Res*. 2011; 469(6):1525-7.

12. Bufquin T, Hersan A, Hubert L, Massin P. Reverse shoulder arthroplasty for the treatment of three- and four-part fractures of the proximal humerus in the elderly: a prospective review of 43 cases with a short-term follow-up. *J Bone Joint Surg* Br. 2007 Apr; 89(4):516-20.

13. Day JS, MacDonald DW, Olsen M, Getz C, Williams GR, Kurtz SM. Polyethylene wear in retrieved reverse total shoulder components *J Shoulder Elbow Surg.* 2012; 21:667-674.

14. Drake GN, O'Connor DP, Edwards TB. Indications for reverse total shoulder arthroplasty in rotator cuff disease. *Clin Orthop Relat Res*. 2010 Jun;468(6):1526-33.

15. Ecklund KJ, Lee TQ, Tibone J, Gupta R. Rotator cuff tear arthropathy. *The Journal of the American Academy of Orthopaedic Surgeons*. 2007; 15:340-349.

16. Falaise V, Levigne C, Favard L. Incidence des encoches du pilier de la scapula des prothèses totales inversées de l'épaule : influence de l'angle glénométaphysaire. *Rev Chir Ortho Trauma*. 2011; 97(6):S233-S239

17. Faro Technologies. *Faro Laser ScanArm Edge: Manual.* Lake Mary, FL: Faro Technologies Inc. 2014

18. Farshad M, Gerber C. Reverse total shoulder arthroplasty-from the most to the least common complication. *Int Orthop*. 2010; 34(8):1075-82.

53

19. Feeley BT, Gallo RA, Craig EV. Cuff tear arthropathy: current trends in diagnosis and surgical management. *J Shoulder Elbow Surg*. 2009 May-Jun; 18(3):484-94.

20. Ferrel, JR, Trinh, TQ, Fischer RA. Reverse Total Shoulder Arthroplasty Versus Hemiarthroplasty for Proximal Humeral Fractures. *Journal of Orthopaedic Trauma*. 2015; 29(1), 60–68.

21. Flatow EL, Harrison AK. A history of reverse total shoulder arthroplasty. *Clin Orthop Relat Res*. 2011; 469(9):2432-9.

22. Friedman RJ, Flurin PH, Wright TW, Zuckerman JD, Roche CP. Comparison of reverse total shoulder arthroplasty outcomes with and without subscapularis repair. *J Shoulder Elbow Surg*. 2017 Apr; 26(4):662-668.

23. Guery J, Favard L, Sirveaux F, Oudet D, Mole D, Walch G. Reverse total shoulder arthroplasty. Survivorship analysis of eighty replacements followed for five to ten years. *The Journal of Bone and Joint Surgery American.* 2006; 88:1742-1747.

24. Guettler JH, Basamania CJ. Muscle transfers involving the shoulder. J *Surg Orthop Adv*. 2006; 15(1):27-37.

25. Holcomb JO, Cuff D, Petersen SA, Pupello DR, Frankle MA. Revision reverse shoulder arthroplasty for glenoid baseplate failure after primary reverse shoulder arthroplasty. *J Shoulder Elbow Surg*. 2009; Sep-Oct; 18(5):717-23.

26. Hyun YS, Huri G, Garbis NG, McFarland EG. Uncommon indications for reverse total shoulder arthroplasty. *Clin Orthop Surg*. 2013; 5(4):243-55.

27. Iannotti JP, Gabriel JP, Schneck SL, Evans BG, Misra S. The normal glenohumeral relationships. An anatomical study of one hundred and forty shoulders. *J Bone Joint Surg Am*. 1992 Apr; 74(4):491-500.

28. Jazayeri R, Kwon YW. Evolution of the reverse total shoulder prosthesis. *Bull NYU Hosp Jt Dis*. 2011; 69(1):50-5.

29. Jensen KL, Williams GR, Russell IJ, Rockwood CA. Rotator cuff tear arthropathy. J Bone Joint Surg Am 1999; 81:1312-24.

30. Ji S, Ford JC, Greenwald RM, et al. Automated subject-specific, hexahedral mesh generation via image registration. *Finite Elem Anal Des*. 2011;47(10):1178-1185.

31. Katz D, O'Toole G, Cogswell L, Sauzieres P, Valenti P. A history of the reverse shoulder prosthesis. *Int J Shoulder Surg*. 2007; 1:108-13.

32. Khadilkar L, MacDermid JC, Sinden KE, Jenkyn TR, Birmingham TB, Athwal GS. An analysis of functional shoulder movements during task performance using Dartfish movement analysis software. *Int J Shoulder Surg*. 2014 Jan;8(1):1-9.

33. Khair MM, Gulotta LV. Treatment of irreparable rotator cuff tears. *Curr Rev Musculoskelet Med.* 2011; 4: 208–13.

34. Kim SH, Wise BL, Zhang Y, & Szabo RM. Increasing incidence of shoulder arthroplasty in the United States 2011. *The Journal of Bone & Joint Surgery*. 2011; 93(24), 2249-2254.

35. Lee JH, Chun MH, Jang DH, Ahn JS, Yoo JY. A comparison of young and old using three-dimensional motion analyses of gait, sit-to-stand and upper extremity performance. *Aging Clin Exp Res*. 2007 Dec; 19(6):451-6.

36. Lugo R, Kung P, Ma CB. Shoulder biomechanics. *Eur J Radiol*. 2008 Oct;68(1):16-24.

37. Martelli S, Bignozzi S, Bontempi M, et al. Comparison of an optical and a mechanical navigation system. *Lect Notes Comput Sci*. 2003; 2879 (part 2):303–310.

54

38. McCluskey, George M., Howard D. Routman and DO Director. "The Deltopectoral Approach for Reverse Shoulder Arthroplasty." *The St. Francis Orthopaedic Institute Scientific Bulletin*. 2011; 3(7).

39. Mochizuki T, Sugaya H, Uomizu M, Maeda K, Matsuki K, Sekiya I, Muneta T, Akita K. Humeral insertion of the supraspinatus and infraspinatus. New anatomical findings regarding the footprint of the rotator cuff. *J Bone Joint Surg Am*. 2008 May; 90(5):962-9.

40. Molé D, Wein F, Dézaly C, Valenti P, Sirveaux F. Surgical technique: the anterosuperior approach for reverse shoulder arthroplasty. *Clin Orthop Relat Res*. 2011; 469(9):2461-8.

41. Nam D, Kepler CK, Neviaser AS, Jones KJ, Wright TM, Graig EV, Warren RF. Reverse total shoulder arthroplasty: current concepts, results, and component wear analysis. *The Journal of Bone and Joint Surgery*. 2010; 23-35

42. Namdari S, Yagnik G, Ebaugh DD, Nagda S, Ramsey ML, Williams GR Jr, Mehta S. Defining functional shoulder range of motion for activities of daily living. *J Shoulder Elbow Surg*. 2012 Sep; 21(9):1177-83:148-160

43. Neer CS, Craig EV, Fukuda H. Cuff-tear arthropathy. *J Bone Joint Surg Am*. 1983; 65:1232–1244.

44. Oliveira BL, Sundnes J. Comparison of tetrahedral and hexahedral meshes for finite element simulation of cardiac electro-mechanics. *VII European Congress on Computational Methods in Applied Sciences and Engineering*. 2016; M. Papadrakakis, V. Papadopoulos, G. Stefanou, V. Plevris (eds.). National Technical University of Athens.

45. Oosterwijk AM, Nieuwenhuis MK, van der Schans CP, Mouton LJ. Shoulder and elbow range of motion for the performance of activities of daily living: A systematic review. *Physiotherapy Theory and Practice*. 2018; 34(7)L:505-528.

46. Permeswaran VN, Goetz JE, Rudert MJ, Hettrich CM, Anderson DD. Cadaveric validation of a finite element modeling approach for studying scapular notching in reverse shoulder arthroplasty. *Journal of Biomechanics* 2016; Sep 6;49(13):3069-3073.

47. Permeswaran VN, Caceres AP, Goetz JE, Anderson DD, Hettrich CM. The effect of glenoid component version and humeral polyethylene liner rotation on subluxation and impingement in reverse shoulder arthroplasty. *J Shoulder Elbow S*. 2017 Oct; 26(10):1718-1725.

48. Permeswaran VN. Development of a computational model to study instability and scapular notching in reverse shoulder arthroplasty. PhD thesis, University of Iowa. 2017.

49. Quental C, Fernandes P, Monteiro J, Folgado J. Bone remodelling of the scapula after a total shoulder arthroplasty. *Biomechanics and Modeling in Mechanobiology*. 2014; 13(4):827–838.

50. Rainsberger R. TrueGrid User's Manual. *XYZ Scientific Applications Inc*. 2006; 2(3).

51. Randelli P, Randelli F, Compagnoni R, Cabitza P, Ragone V, Pulici L, Banfi G. Revision reverse shoulder arthroplasty in failed shoulder arthroplasties for rotator cuff deficiency. *Joints*. 2015 Jun 8; 3(1):31-7.

52. Rundquist PJ, Obrecht C, Woodruff L. Three-dimensional shoulder kinematics to complete activities of daily living. *Am J Phys Med Rehabil*. 2009 Aug;88(8):623-9.

53. Samitier G, Alentorn-Geli E, Torrens C, Wright TW. "Reverse shoulder arthroplasty. Part 1: systematic review of clinical and functional outcomes." *International Journal of Shoulder Surgery*. 2015; 24-31.

54. Soslowsky LJ, Carpenter JE, Bucchieri JS, Flatow EL. Biomechanics of the rotator cuff. *Orthop Clin North Am*. 1997; Jan; 28(1):17-30.

55. Stanbury SJ, Voloshin I. Reverse Shoulder Arthroplasty for Acute Proximal Humeral Fractures in the Geriatric Patient. *Ger Ortho Surg Rehab*. 2012; 2(5-6):181-186.
56. Tadepalli SC, Erdemir A, Cavanagh PR. Comparison of hexahedral and tetrahedral elements in finite element analysis of the foot and footwear. *J Biomech*. 2011 Aug 11; 44(12):2337-43.
57. Theodossy T, Bamber MA. Model surgery with a passive robot arm for orthognathic surgery planning. *J Oral Maxillofac Surg*. 2003; 61:1310-1317.
58. Vu AF, Chundury RV, Perry JD. Comparison of the FaroArm Laser Scanner with the MicroScribe Digitizer Using Basicranial Measurements. *J Craniofac Surg*. 2017 Jul; 28(5):e460-e463.
59. Walker M, Brooks J, Willis M, Frankle M. How reverse shoulder arthroplasty works. *Clinical Orthopaedics and Related Research.* 2011; 2440-2451.
60. Webb JD, Blemker SS, Delp SL. 3D finite element models of shoulder muscles for computing lines of actions and moment arms. *Comput Methods Biomech Biomed Engin*. 2014; 17(8):829-37.
61. Westermann RW, Pugely AJ, Martin CT, Gao Y, Wolf BR, Hettrich CM. Reverse shoulder arthroplasty in the United States: a comparison of national volume, patient demographics, complications, and surgical indications. *Iowa Orthop J*. 2015; 35:1-7.
62. Zheng M, Zou Z, Bartolo PJ, Peach C, Ren L. Finite element models of the human shoulder complex: a review of their clinical implications and modelling techniques. *Int J Numer Method Biomed Eng*. 2017 Feb; 33(2).
63. Zilber S. Shoulder Arthroplasty: Historical Considerations. *Open Orthop J*. 2017; 11:1100-1107.
64. Zimmer. *Zimmer Trabecular Metal Reverse Shoulder System surgical technique: Manua*l. Zimmer. 2012.
65. Zumstein MA, Pinedo M, Old J, Boileau P. Problems, complications, reoperations, and revisions in reverse total shoulder arthroplasty: a systematic review. *J Shoulder Elbow S*. 2011; 20:146-157.